5 Results and Discussion

5.1 HPLC analytical method development for simultaneous estimation of VRL and RES

5.1.1 Identification of λmax for VRL and RES

VRL and RES at concentration of 10 µg mL^{-1} was scanned in double beam U.V visible spectrophotometer in mobile phase (acetonitrile (60 %) and 50 mM phosphate buffer (40 %, with 1 % triethyamine), pH 3.5, (pH adjusted with orthophosphoric acid)) and PBS, pH 7.4 between the scanning range 200 to 400 nm to determine λmax. The λmax values for VRL and RES were found to be 278 nm and 306 nm, respectively.

5.1.2 Calibration curve

20 µL of the standard solutions of VRL and RES were injected in to the HPLC and corresponding peak areas were measured at 268 and 306 nm for VRL and RES, respectively. The calibration curve was prepared by plotting peak area vs. concentration (µg mL^{-1}) as shown in Figure 5.1 and 5.2 for VRL and RES, respectively. Beer Lambert's law was followed in the concentration range of 5-100 µg mL^{-1} and 10- 5000 ng $mL^{-1}$for VRL and RES, respectively. The straight line regression equations for VRL and RES are given in Table 5.1. The value of R^2 indicated high linearity between peak area and concentration.

Table 5.1: Regression equations and R^2 value of calibration curves in different solvents

Drug	**In water**		**In PBS, 7.4**	
	Regression Equation	**R^2**	**Regression Equation**	**R^2**
VRL	y = 19114x - 1237	0.999	y = 13555x - 6688	0.999
RES	y = 13393x + 1800	0.999	44646x + 600.2	0.999

(a)

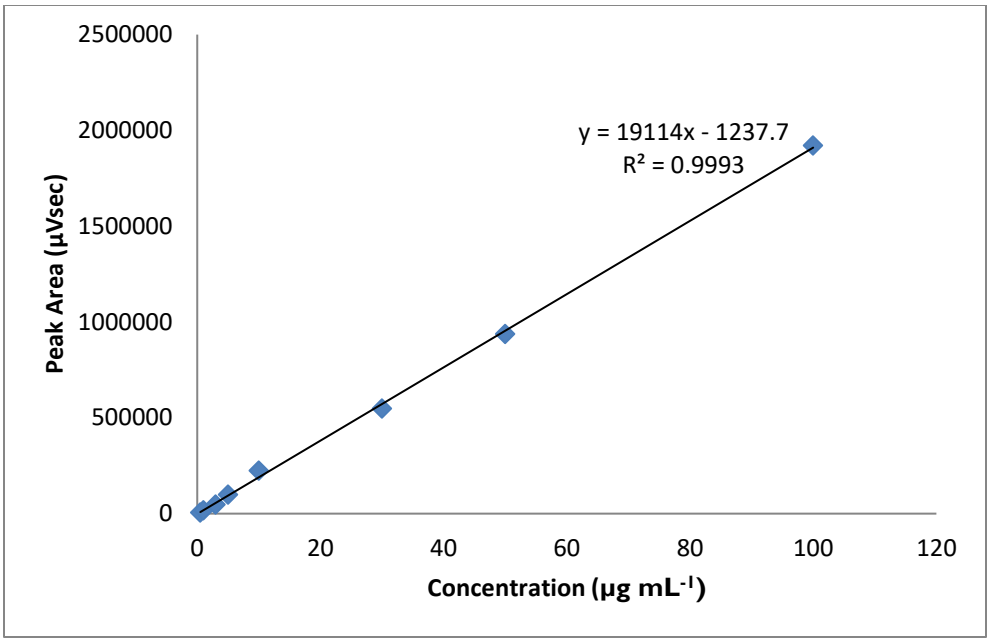

(b)

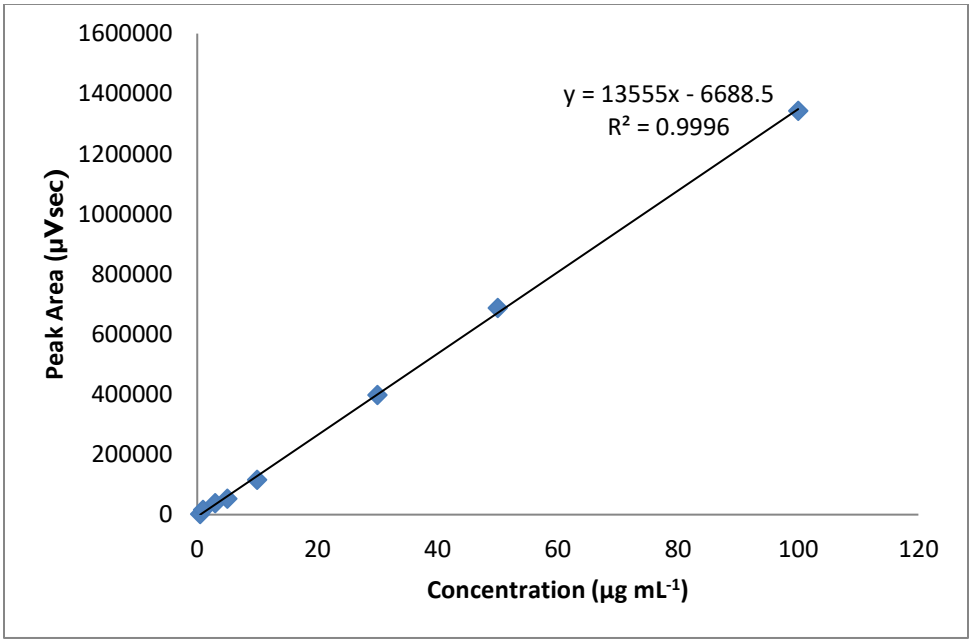

Figure 5.1: Calibration curve of VRL in (a) mobile phase and (b) PBS, pH 7.4

(a)

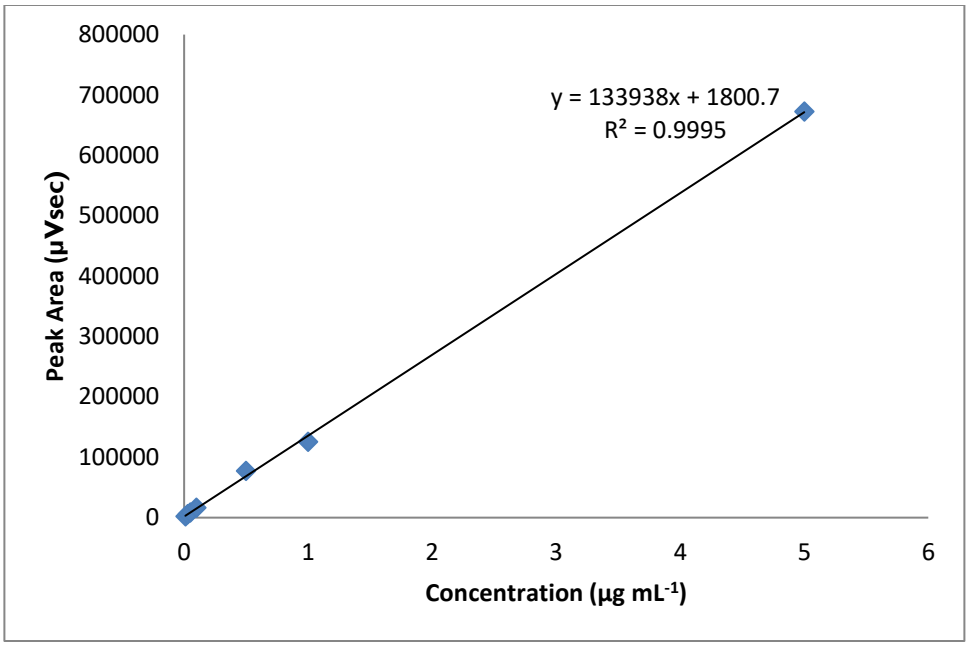

(b)

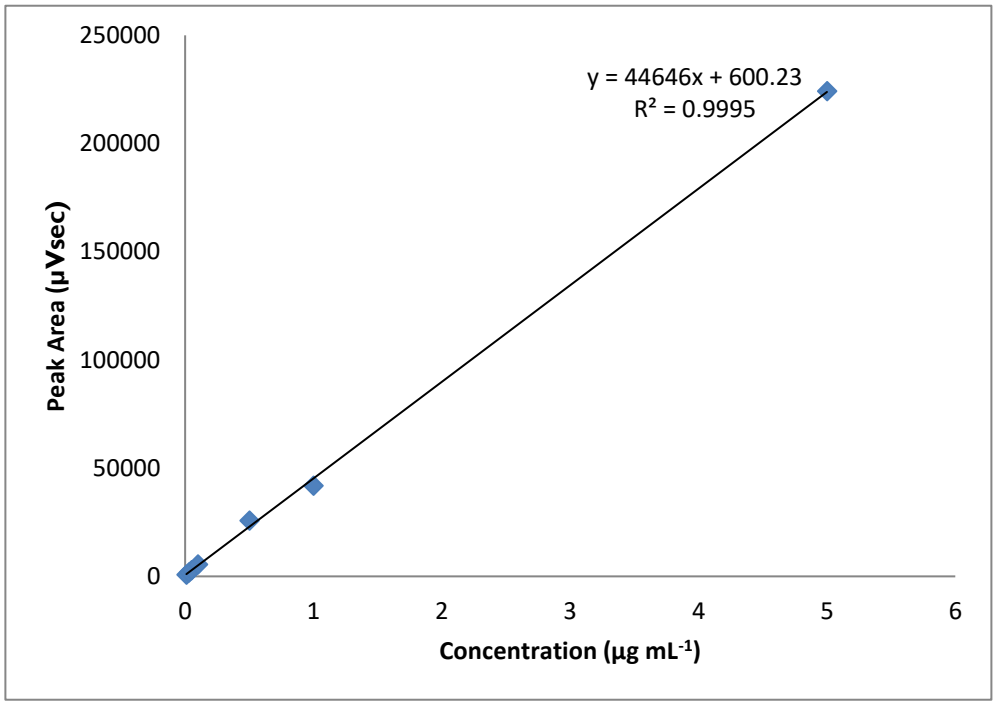

Figure 5.2: Calibration curve of RES in (a) mobile phase and (b) PBS, pH 7.4

5.1.3 Method validation

Typical chromatogram of VRL and RES obtained by HPLC is shown in Figure 5.3. The specificity of the RP-HPLC method was determined by comparing the chromatogram of mixed standards. The parameters like retention time (Rt), resolution (Rs) and tailing factor (Tf) were calculated (Table 5.2). Good correlation was obtained between the results of mixed standards and sample solutions.

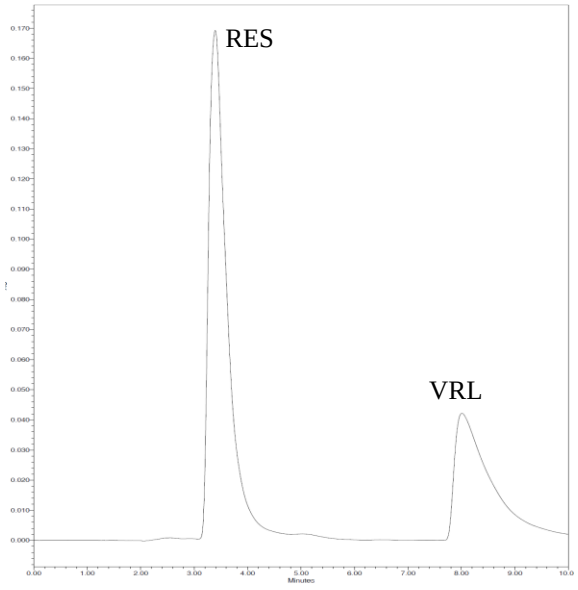

Figure 5.3: Typical chromatogram of VRL (Rt=8.24 min) and RES (Rt=3.4 min).

Table 5.2: Parameters for assessing specificity of the analytical method

Parameters	**VRL**	**RES**
Retention time, Rt	8.24 min	3.4 min
Resolution, Rs	4.4	
Tailing factor, Tf	1.67	1.16
Capacity factor	2.01	7.24

Recovery studies were performed for determination of accuracy of the developed method for estimation of VRL and RES in mobile phase and PBS, pH 7.4. The variability associated with the developed analytical method in different media was measured by determining precision (intra-day and inter-day). Three concentrations (low, medium and high) were selected. Each concentration was scanned in the HPLC at same day (n=3) and over three consecutive days (n=3) to access intra-day and inter-day variation, respectively. The results of intra-day and inter-day variability in water and PBS, pH 7.4 are summarized in Table 5.3 and Table 5.4, respectively. Results were within specified limits of less than 15 % for all the three different concentrations.

Table 5.3: The intra-day and inter-day variability of the analytical method for VRL

Actual conc.(µg mL^{-1})	**In water**			**In PBS, pH 7.4**		
	5	**10**	**50**	**5**	**10**	**50**
Intra-day Variation						
Calculated conc.(µg mL^{-1})	5.12 ± 0.13	10.15 ± 0.27	49.89 ± 0.64	5.05 ± 0.24	9.91 ± 0.42	50.4 ± 0.66
Recovery (%)	102.3 ± 2.70	101.5 ± 2.71	98.3 ± 1.21	101 ± 4.76	99.1 ± 4.20	100.9 ± 1.33
%RSD	2.64	2.68	1.29	4.71	4.24	1.32
% bias	2.0	5.0	-0.2	1.00	-0.90	0.09
Inter-day variation						
Calculated conc.(µg mL^{-1})	5.09 ± 0.11	9.99 ± 0.26	50.34 ± 0.90	4.92 ± 0.15	10.1 ± 0.34	50.12 ± 0.22
Recovery (%)	101.8 ± 2.2	99.9 ± 2.6	100.6 ± 1.8	98.4 ± 3.3	100.1 ± 3.40	100.6 ± 0.45
%RSD	2.16	2.66	1.79	3.18	3.41	0.44
% bias	1.8	-0.06	-0.07	-1.5	1.3	0.24

Table 5.4: The intra-day and inter-day variability of the analytical method for RES

Actual conc.(ng mL^{-1})	**In water**			**In PBS, pH 7.4**		
	5	**10**	**50**	**5**	**10**	**50**
Intra-day Variation						
Calculated conc.(ng mL^{-1})	5.02 ± 0.15	10.07 ± 0.29	50.51 ± 1.36	5.04 ± 0.17	9.97 ± 0..15	50.8 ± 1.3
Recovery (%)	100.5 ± 3.1	100.7 ± 2.9	101.0 ± 2.7	100.9 ± 3.5	98.6 ± 5.0	99.7 ± 1.75
%RSD	3.09	2.9	2.7	3.55	1.7	2.6
% bias	0.53	0.7	1.02	0.9	-0.3	1.6
Inter-day variation						
Calculated conc.(ng mL^{-1})	5.06 ± 0.51	9.97 ± 0.34	49.51 ± 3.94	5.1 ± 0.36	9.86 ± 0.5	49.2 ± 3.84
Recovery (%)	101.3 ± 1.30	99.7 ± 3.89	99.02 ± 2.88	101.9 ± 7.1	98.6 ± 5.0	98.4 ± 4.33
%RSD	10.3	3.89	7.6	7.0	5.08	7.8
% bias	1.3	-0.3	-0.98	1.93	-1.4	-1.6

The consistency of results on same day as well as different days confirmed that the developed analytical method is accurate and reproducible for the measurement of VRL and RES in water and PBS, pH 7.4. The low variability in the results indicated the suitability of analytical method for consistent and efficient analysis during *in-vitro* analyses. The LOD, and LOQ of VRL and RES in different media are given in Table 5.5.

Table 5.5: LOD and LOQ of VRL and RES in water and PBS, pH 7.4

Drug	**In water**		**In PBS, pH 7.4**	
	LOD	**LOQ**	**LOD**	**LOQ**
VRL	4.2 µg mL^{-1}	12.7 µg mL^{-1}	5.04 µg mL^{-1}	15.2 µg mL^{-1}
RES	5.03 ng mL^{-1}	15.1 ng mL^{-1}	1.3 ng mL^{-1}	4.12 ng mL^{-1}

5.2 Preliminary screening

Preliminary results indicated that GMO was found to display maximum loading efficiency of about 52.13 % followed by GMS and PLGA which showed 34.5 % and 19.8 % loading efficiency, respectively. Therefore, GMO was selected for preparation of nanoparticles.

5.3 Solid lipid nanoparticles (SLNs)

5.3.1 Experimental design

Taguchi orthogonal design was utilized to prepare 9 batches of TPGS-VRL-SLNs and PL-VRL-SLNs using concentration of lipid (X_1), concentration of surfactant (X_2) homogenization speed (X_3) and homogenization time (X_4) as independent variables, analyzed for all possible combinations and their influence on dependent variables particle size and entrapment efficiency were evaluated (Table 5.6). The generated equations depicted the relationship of the variables on the measured response. The positive coefficient of the factor in polynomial equation suggested direct relationship, whereas the negative coefficient indicated inverse relationship. The influence of interactions between variables on response was studied by generating three-dimensional surface graphs (Figure 5.4 and Figure 5.5) (Mishra et al., 2017, Patel et al., 2016, Vardhan et al., 2017).

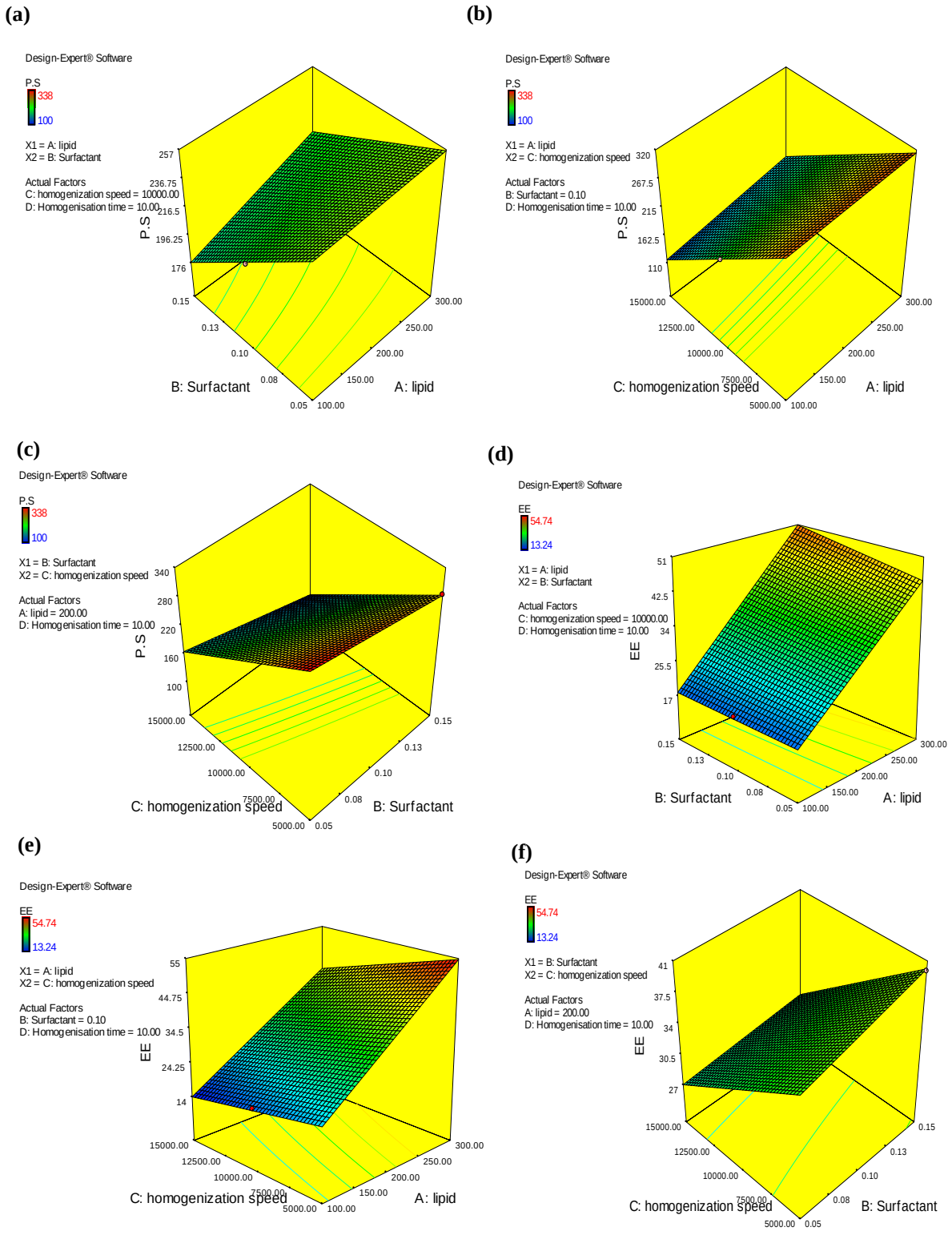

Figure 5.4: Three-dimensional response surface plots showing the effect of independent variables (concentration of lipid, concentration of surfactant and homogenization speed) on response variables. P.S: particle size (a, b, c) and EE: entrapment efficiency (d, e, f) of TPGS-VRL-SLNs

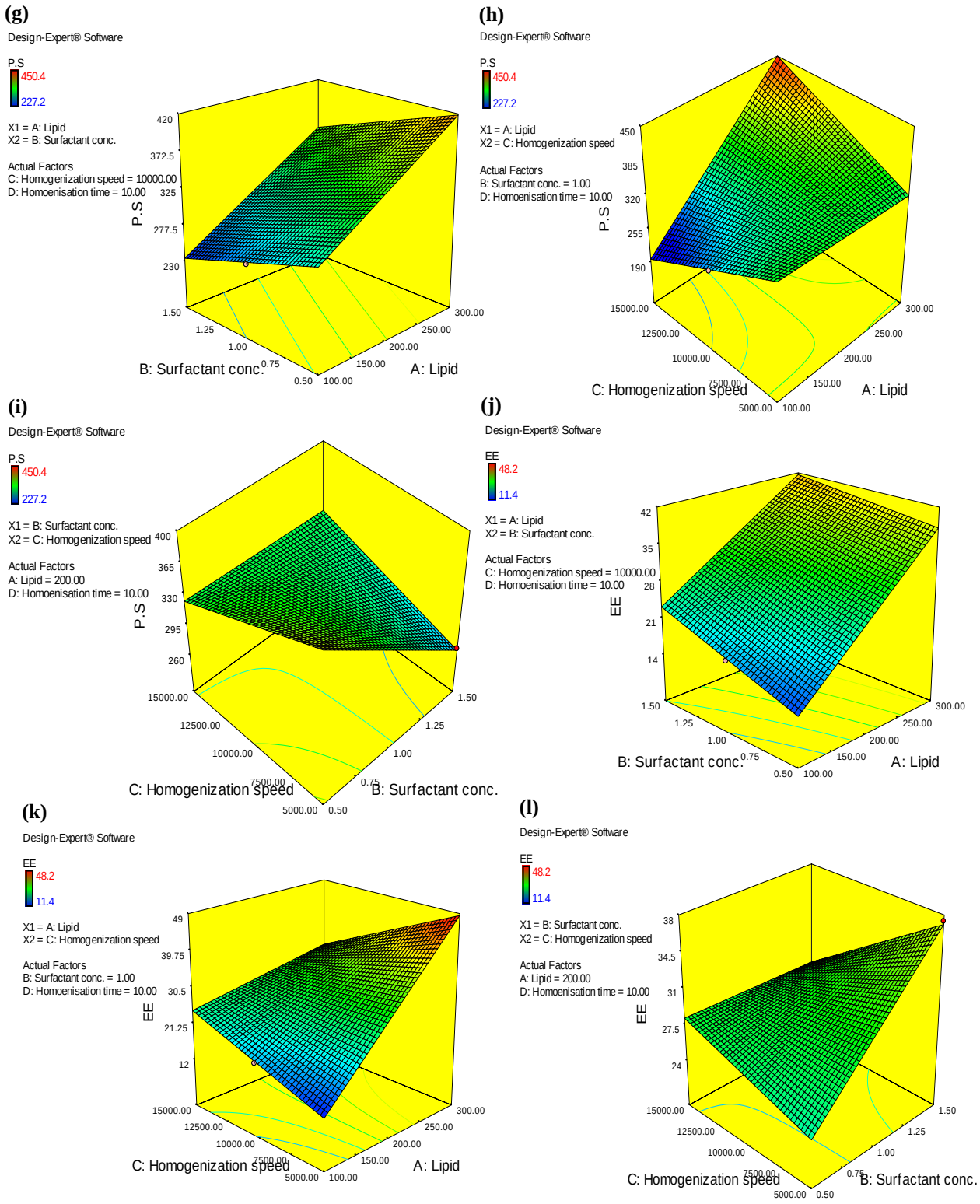

Figure 5.5: Three-dimensional response surface plots showing the effect of independent variables (concentration of lipid, concentration of surfactant and homogenization speed) on response variables. P.S: particle size (g, h, i) and EE: entrapment efficiency (j, k, l) of PL-VRL-SLNs

Table 5.6: Taguchi experimental design showing experimental runs with independent variables and their measured responses: Particle size and entrapment efficiency. Values are represented as mean ± S.D, n=3

Runs	Independent variables				Dependent variables			
					TPGS-VRL-SLNs		PL-VRL-SLNs	
	X_1	X_2	X_3	X_4	P.S (nm)	EE (%)	P.S (nm)	EE (%)
1	3	2	1	3	338.0 ± 2.3	54.7 ± 2.1	352.9 ± 1.2	41.7 ± 3.2
2	1	1	1	1	321.0 ± 6.3	21.6 ± 3.4	367.4 ± 4.3	11.4 ± 2.1
3	2	3	1	2	287.0 ± 3.2	39.9 ± 1.2	267.4 ± 2.6	37.4 ± 4.1
4	2	2	3	1	112.0 ± 2.1	27.6 ± 5.3	293.4 ± 3.2	35.0 ± 2.3
5	3	3	2	1	187.0 ± 7.4	51.1 ± 1.2	321.9 ± 2.3	48.2 ± 1.2
6	1	2	2	2	212.0 ± 5.4	18.5 ± 2.2	262.7 ± 2.2	18.2 ± 3.1
7	3	1	3	2	178.0 ± 4.6	39.4 ± 5.3	450.4 ± 3.2	32.8 ± 2.5
8	1	3	3	3	100.0 ± 9.3	13.2 ± 2.3	227.2 ± 2.2	19.4 ± 1.0
9	2	1	2	3	278.0 ± 3.4	31.4 ± 1.1	390.7 ± 1.1	19.7 ± 1.2

5.3.1.1 Influence of independent variables on particle size.

Particle size of TPGS-VRL-SLNs was found to be in the range of 100.0 ± 4.3 to 338.1 ± 2.3 nm whereas PL-VRL-SLNs ranged from 227.4 ± 3.2 to 450.4 ± 6 nm, respectively. TPGS concentration was 10 times lower than PL-188 inspite of that TPGS emulsified SLNs showed lower particle size than emulsified SLNs. This indicates the excellent emulsification efficiency of TPGS. The mathematical polynomial equations with constants and regression coefficients generated by multiple linear regressions for particle size (Y_1) were given as:

$$Y_{1\ (TPGS\text{-}VRL\text{-}SLN)} = 223.67 + 9.95\ X_1 - 29.98\ X_2 - 89.02\ X_3 + 23.50\ X_4 + 7.29\ X_1X_2 + 7.71X_1X_3 - 3.43\ X_2X_3 \quad \text{Equation 5.1}$$

$$Y^*_{1\ (PL\text{-}VRL\text{-}SLN)} = 326 + 60.21\ X_1 - 31.99\ X_2 - 2.98\ X_3 + 31.17\ X_4 - 0.39\ X_1X_2 + 66.69\ X_1X_3 + 31.13\ X_2X_3 \quad \text{Equation 5.2}$$

The linear model for TPGS-VRL-SLN with F value of 642.79 and p values of < 0.0001 suggested best fit for particle size. The value of coefficient (R^2) was found to be 0.9984, indicating a good fit between predicted values and experimental values. Similarly for PL-VRL-SLNs a linear model showing F value of 13.75, p value of < 0.05 and R^2 value of 0.9322 is also good fit for particle size. Hence, the models can be used to navigate the design space (Joshi et al., 2010, Patel et al., 2016, Solanki et al., 2007).

Concentration of lipid in formulation has significant effect on the particle size of the SLN. It affects particle size positively in both TPGS-VRL-SLNs, and PL-VRL-SLNs (Equation 3 & 4). The same can be seen in Figure 5.4 (a) and Figure 5.5 (g). Higher lipid concentration imparts viscosity to the dispersed phase which will reduce the stirring efficacy and pose resistance to droplet breakdown, resulting in larger particles (Mishra et al., 2014, Patel et al., 2016).

Surfactant concentration inversely affects particle size (Equation 5.1 & 5.2) for both TPGS-VRL-SLNs and PL-VRL-SLNs which might be attributed to the production and stabilization of smaller lipid droplets at higher surfactant concentration as enough amount of surfactant was present to stabilize the SLN (Mishra et al., 2014, Vuddanda et al., 2015). The smaller-size particles formed with increased surfactant concentration (Figure 5.4 (a) and Figure 5.5 (g)) might be the consequence of reduced interfacial tension between organic and aqueous phases, which eventually forms smaller-sized droplets (Singh et al., 2014). Moreover, type of surfactant also affects particle size as TPGS-VRL-SLN particles were found to be much smaller than that of PL-VRL-SLN which can be also explained on the basis of lower critical micelle concentration (CMC) of TPGS (0.02 %) compared to PL-188 (0.04 %).

Homogenization speed also affects particle size negatively (Equation 5.1 & 5.2) but the effect was found to be more pronounced for TPGS-VRL-SLNs (Figure 5.4 (b) and Figure 5.5 (k)). The decrease in particle size can be attributed to high intensity shear forces which can overcome the intra-particle forces and resulted in small particles (Anarjan et al., 2015, Kushwaha et al., 2013).

Homogenization time affects the particle size positively in both TPGS-VRL-SLNs and PL-VRL-SLNs (Equation 5.1 & 5.2). The increase in particle size with increase in homogenization time can be attributed to development of more surface free energy, at higher homogenization speed, which can cause coalescence of particles (Anarjan et al., 2015).

5.3.1.2 Influence of independent variables on EE

The EE of TPGS-VRL-SLNs and PL-VRL-SLNs varies in the range of 18.5 ± 2.2 % to 54.7 ± 2.1 % and 11.4 ± 2.1 % to 48.2 ± 1.2 %, respectively, for various factor's level combinations. The effect of the independent variables on EE can be explained by the following formula:

$$Y_{2\ (TPGS\text{-}VRL\text{-}SLN)} = 33.07 + 15.07\ X_1 - 1.32\ X_2 - 5.26\ X_3 - 0.11\ X_4 + 1.44\ X_1 X_2 - 1.32\ X_1 X_3 - 0.53\ X_2 X_3 \quad \text{Equation 1.3}$$

$$Y^*_{2\ (PL\text{-}VRL\text{-}SLN)} = 326 + 60.21\ X_1 - 31.99\ X_2 - 2.98\ X_3 + 31.17\ X_4 - 0.39\ X_1 X_2 + 66.69\ X_1 X_3 + 31.19 X_2 X_3 \quad \text{Equation 5.4}$$

The linear models with F values (416.33 and 13.75), p values (< 0.001 and < 0.05) and R^2 values (0.9976 and 0.9322) for TPGS-VRL-SLNs and PL-VRL-SLNs, respectively, indicating a good fit and model adequacy.

As more lipid and inter lipid space is available for encapsulation of VRL molecules, EE was found to be increased (Equation 5.3 & 5.4). Increased lipid concentration also restricts the

outward movement of hydrophilic drug towards the external aqueous phase by imparting viscous diffusional barrier at the interface, leading to an increase in EE (Mishra et al., 2014, Patel et al., 2016). The effect of lipid concentration is shown in Figure 5.4 (a) and Figure 5.5(g).

The surfactant concentration was related inversely (Equation 5.3 & 5.4) with EE. This could be explained by marked reduction in interfacial tension, which ultimately increases drug partition into aqueous phase, contributing to substantial lowering of the EE (Patel et al., 2016). Homogenization speed and time were found to have negligible effect on EE. However, for PL-VRL-SLNs EE was found to be increased with homogenization time this can be attribute to marked increase in particle size which can accommodate more VRL.

5.3.2 Determination of optimal conditions for preparation of TPGS-VRL-SLNs and PL-VRL-SLNs

Desirability approach was utilized simultaneously for numerical optimization of responses, such as particle size and entrapment efficiency, to obtain optimized TPGS-VRL-SLNs and PL-VRL-SLNs. Constraints were applied and the levels of independent variables to obtain the optimum response were determined. The new batch was prepared with predictive levels of independent variables and evaluated for prediction error to validate the optimization process. The desirability of optimized batches of TPGS-VRL-SLN and PL-VRL-SLN were found to be 0.996 and 0.998, respectively. The selected levels of various independent variables are shown in Table 5.7. The optimized batch for TPGS-VRL-SLNs and PL-VRL-SLNs were prepared and the experimental values were found to be very close to predicted values.

Table 5.7: Optimized batch with measured responses using desirability approach. All results are presented as mean ± SD; n=3.

Variables	**Optimized value**			
	TPGS-VRL-SLNs		**PL-VRL-SLNs**	
Lipid concentration (X_1)	300		293	
Surfactant concentration (X_2)	0.15		1.5	
Homogenization speed (X_3)	6531		5000	
Homogenization time (X_4)	5		5	
Results	**Predicted**	**Experimental**	**Predicted**	**Experimental**
Particle size (nm)	248.9	249.4 ± 8.1	228	234.6 ± 9.2
EE (%)	55.8	55.3 ± 2.3	59.2	58.4 ± 2.1
PDI	0.2 ± 0.1		0.3 ± 0.1	
Zeta Potential (mV)	-10.6 ± 2.1		-11.0 ± 0.4	

5.3.3 Characterization of VRL-SLNs

5.3.3.1 Particle size, PDI, and entrapment efficiency

The mean particle size, PDI and EE of the optimized batch of TPGS-VRL-SLN were found to be 249.4 ± 8.1 nm, 0.2 ± 0.1 and 55.3 ± 2.3 %, respectively. For PL-VRL-SLN the respective values were 234.6 ± 9.2 nm, 0.3 ± 0.1 and 58.4 ± 2.1 %, respectively. The observed values of various responses for both VRL-SLNs were found to be very close to that determined experimentally utilizing desirability approach. The prediction error was found to be negligible which suggested the predictability of the model Table 5.7 (Mishra et al., 2017, Patel et al., 2016). The stability of VRL in the VRL-SLNs can be attributed to the presence of single peak at same retention time while determining EE (%) (Bougaret et al., 2005).

5.3.3.2 Zeta potential

Zeta potential is defined by surface charge which in turn is affected by the chemical structure of the molecules involved in the formulation. High absolute value of zeta potential is associated with the stability of the colloidal dispersions. Zeta potential values of TPGS-VRL-SLNs and PL-VRL-SLNs was found to be -10.6 ± 2.1 mV and -11.02 ± 0.4 mV, respectively. Negative charge on TPGS-VRL-SLNs can be attributed to the presence of free carboxyl groups of TPGS (Mishra et al., 2017) which is already proven for its surface modifying properties (Vijayakumar et al., 2016b). The surface layer of the surfactants, i.e., TPGS and poloxamer 188 reduces the surface charge. However, protruding chains (PEG chains of TPGS and polyoxyethylene chains of PL-188) prevent the aggregation of SLNs despite of low value of zeta potential (Mishra et al., 2017).

5.3.3.3 Scanning electron microscopy (SEM)

TPGS-VRL-SLNs and PL-VRL SLNs were found to be spherical in shape. The SEM images are shown in Figure 5.6.

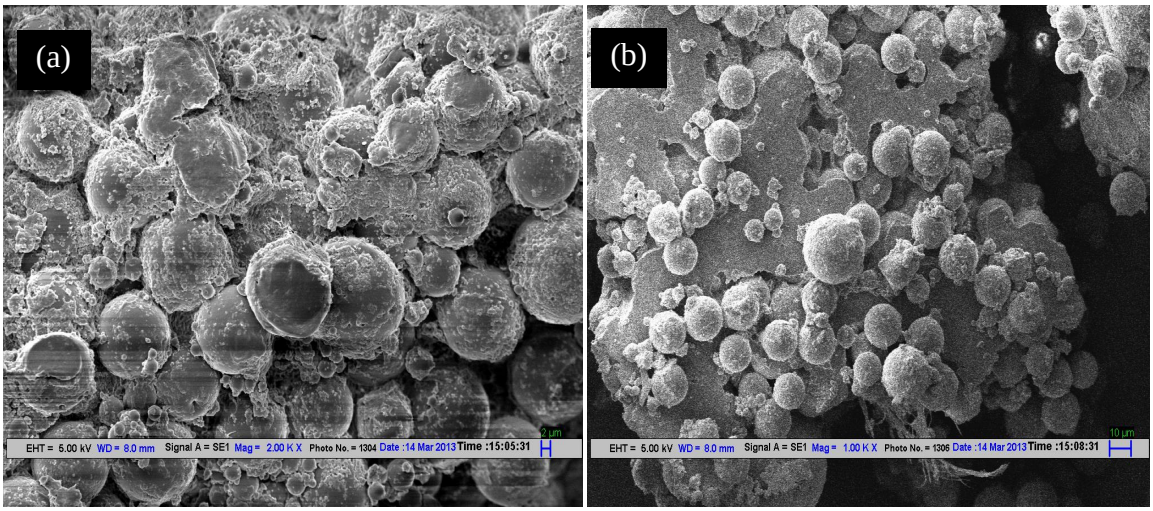

Figure 5.6: Surface morphology by scanning electron microscopy (a) TPGS-VRL-SLNs and (b) PL-VRL-SLNs

5.3.3.4 FTIR

VRL showed its characteristic peaks at 3250-3500 cm^{-1} (corresponds to N-H stretching), 1750 cm^{-1} (carbonyl group of ester).The peaks of VRL in the finger print were well correlated with the peaks obtained from lyophilized TPGS-VRL-SLNs and PL-VRL-SLNs (Figure 5.7). Therefore, there was no chemical change in the drug's identity during preparation of nanoparticles.

5.3.3.5 DSC

The DSC thermograms of VRL showed broad endothermic peaks in the temperature range of 100 - 160 ℃ and 190 – 220 ℃. An exothermic peak was also observed at nearly 250 ℃. The reduced intensity of these peaks suggested absence of any sharp melting point for VRL hence amorphous nature of VRL. The sharp endothermic peak at 56 ℃ in PL-188 thermogram corresponds to its melting point. The broad peaks of TPGS (120 ℃) GMO (30 - 45 ℃)

suggested amorphous nature of TPGS and GMO (Figure 5.8). The thermograms of TPGS-VRL-SLNs and PL-VRL-SLNs displayed the individual peaks of excipients in their original shape with reduction in intensities. This reflects absence of any interaction with VRL. Moreover, the peaks of VRL were not observed in the thermograms which can be attributed to the solubility of VRL in GMO.

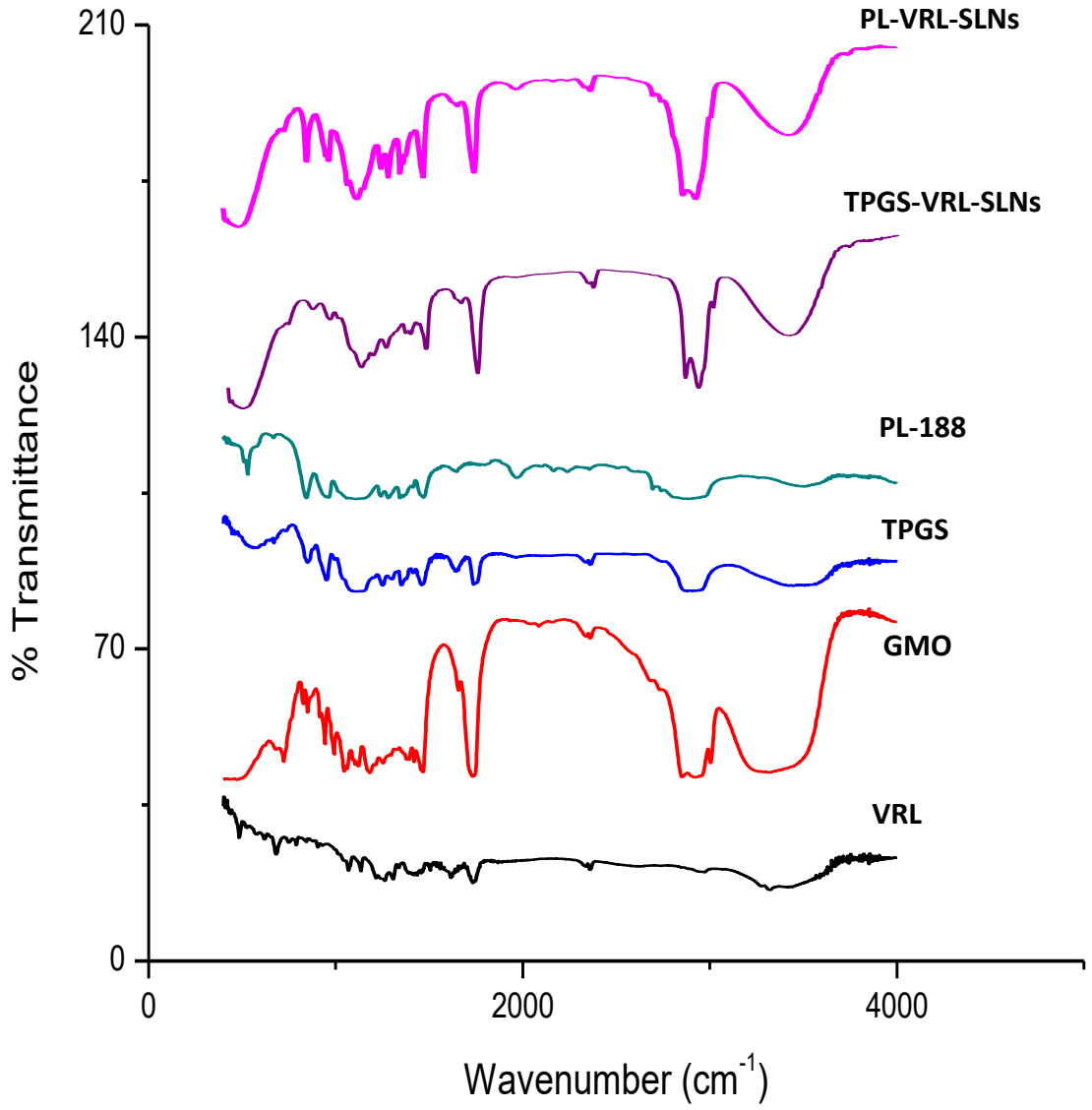

Figure 5.7: FTIR spectra of drug, excipients and lyophilized nanoparticles.

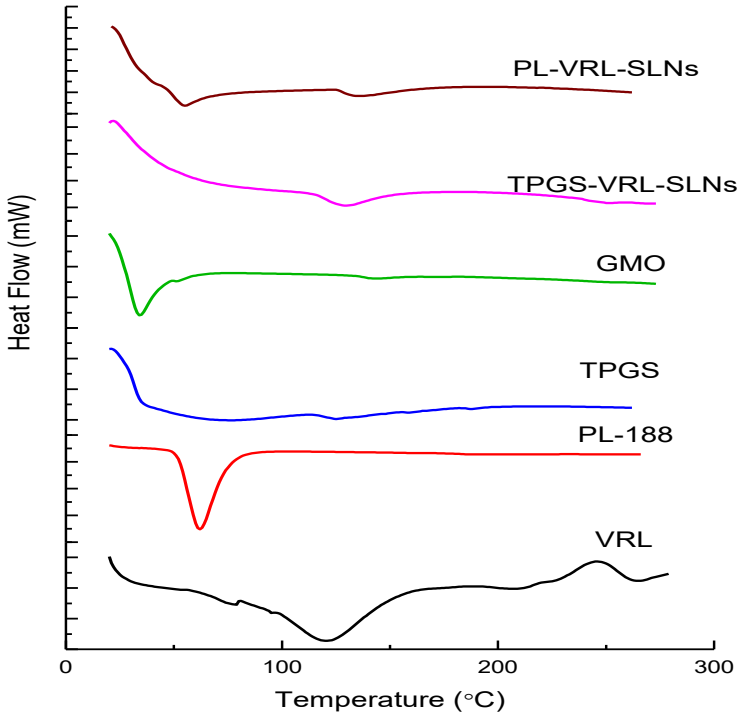

Figure 5.8: DSC thermograms of drug, excipients and lyophilized nanoparticles

5.3.3.6 In vitro drug release studies

The cumulative percentage release data (Figure 5.9) revealed sustained release of drug from TPGS-VRL-SLNs and PL-VRL-SLNs. VRL solution showed 96.7 % in 12 h whereas optimized TPGS-VRL-SLNs and PL-VRL-SLNs showed 68 % and 64 % release in the same time, respectively. TPGS-VRL-SLNs and PL-VRL-SLNs showed burst release of 48 % and 47 %, respectively, in the initial 1 h. The burst release of SLNs can be attributed to the presence of free drug in the SLN suspensions which was further reflected by the encapsulation efficiency. TPGS-VRL-SLNs and PL-VRL-SLNs showed 72 % and 68 % release in 24 h, 83 % and 76 % in 48 h, and 93 % and 89 % in 72 h, respectively. The low

melting point of GMO resulted in the formation of a solid solution upon solidification which provides better control over release of VRL from SLNs (Ekambaram and Sathali, 2011, Zur Mühlen et al., 1998). The slow release of drug from the SLN was due to hydrophobic nature of lipids. PL-VRL-SLNs showed better controlled release profile than TPGS-VRL-SLNs.

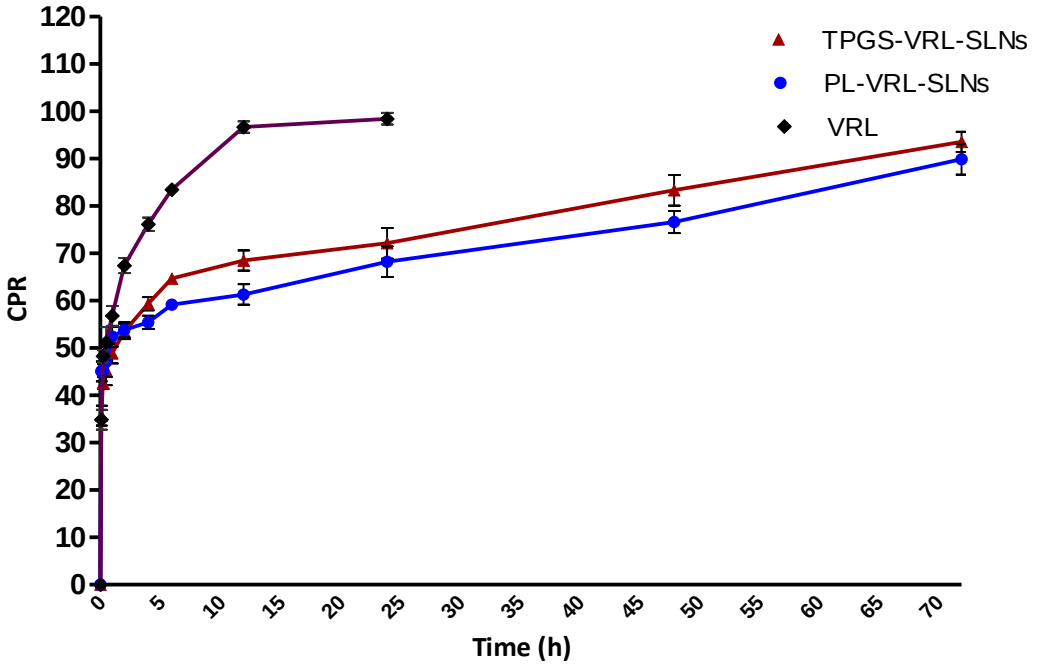

Figure 5.9: Cumulative Percentage Release (CPR) of VRL by VRL solution, TPGS-VRL-SLNs and PL-VRL-SLNs.

Moreover, the release kinetics (Table 5.8) was found to follow Korsemeyer peppas model and n value of < 0.1 which suggests that the release of drug follows super case II transport which confirmed that the mechanism of drug release was erosion controlled.

Table 5.8: Regression co-efficient (R^2) values of optimized TPGS-VRL-SLNs and PL-VRL-SLNs in phosphate buffer pH 7.4

Batch	Zero order	First order	Higuchi	Korsemeyer Peppas
TPGS-VRL-SLNs	0.6458	0.8824	0.8157	0.9952 (n= 0.146)
PL-VRL-SLNs	0.5479	0.7600	0.7102	0.9974 (n= 0.090)

5.3.3.7 Stability studies

The stability studies were performed as per ICH Q1A (R2) guideline. VRL-SLNs were found to be stable without any significant change in the particle size, PDI and EE (Table 5.9). Though the zeta potential of the optimized batches was not found sufficient to stabilize the formulations, stability can be attributed to the steric nature of TPGS and PL-188 which can be due to presence of free carboxyl groups of TPGS and polyoxyethylene chains of PL-188 over nanoparticle surface. The protruding chains prevents aggregation of VRL-SLNs despite of low value of zeta potential (Mishra et al., 2017).

Table 5.9: Particle size (nm) and entrapment efficiency (EE %) and polydispersity index (PDI) of optimized batch of SLNs at different time intervals at room temperature (30 ± 2 ºC/ 60 ± 5% RH). All results are presented as mean ± S.D, n=3.

Parameters		**Days**			
		0	**30**	**60**	**90**
Particle size (nm)	TPGS-VRL-SLNs	249.4 ± 8.1	270.3±2.2	295.3±3.3	302.2±2.1
	PL-VRL-SLNs	234.6 ± 9.2	260.3±2.3	275.3±3.4	287.2±1.2
PDI	TPGS-VRL-SLNs	0.2 ± 0.1	0.4±0.0	0.4±0.0	0.4±0.1
	PL-VRL-SLNs	0.3 ± 0.1	0.3±0.1	0.4±0.0	0.4±0.0
E.E (%)	TPGS-VRL-SLNs	55.3 ± 2.3	49.6±2.5	47.3±3.0	43.4±3.1
	PL-VRL-SLNs	58.5 ± 2.1	52.6±2.4	46.2±3.1	42.5±1.1

5.3.4 *In-vitro* cytotoxicity studies

In-vitro cell line studies were performed on MCF-7 cell lines. 100 µM solutions of VRL, TPGS-VRL-SLNs and PL-VRL-SLNs were prepared in distilled water as stock solutions. From the stock, dilutions were made in the range 0.5 to 50 µM. Cells in conc.1.3 $\times 10^4$ cells per well were incubated in 96 well plated for 48 h and then treated with the prepared dilutions. Placebos of the formulations were taken as positive control during the studies and PBS as negative control. Cell viability was determined with the help of MTT assay and plotted against concentration (Figure 5.10). The IC_{50} values for VRL, TPGS-VRL-SLNs and PL-VRL-SLNs were also determined. IC_{50} value of VRL, TPGS-VRL-SLNs and PL-VRL-SLNs were found to be 19.75, 0.5 and 1.75 µM, respectively. The results of IC_{50} showed that the TPGS-VRL-SLNs and PL-VRL-SLNs are 39.5 and 11.28 fold more effective compared to VRL. Moreover, TPGS-RL-SLNs were found to have significantly more efficacy against MCF-7 cell lines in comparison to PL-VRL-SLNs. The enhanced anticancer activity of TPGS-VRL-SLNs was due to the presence of TPGS. TPGS has been proved to possess anticancer activity by inhibiting efflux of drugs from the cancer cells (Mishra et al., 2017, Vijayakumar et al., 2016b). Moreover, the lipid GMO was found to exhibit fusogenic nature **(ref)** (also depicted by haemolytic studies) which resulted in enormous cell death during *in-vitro* studies.

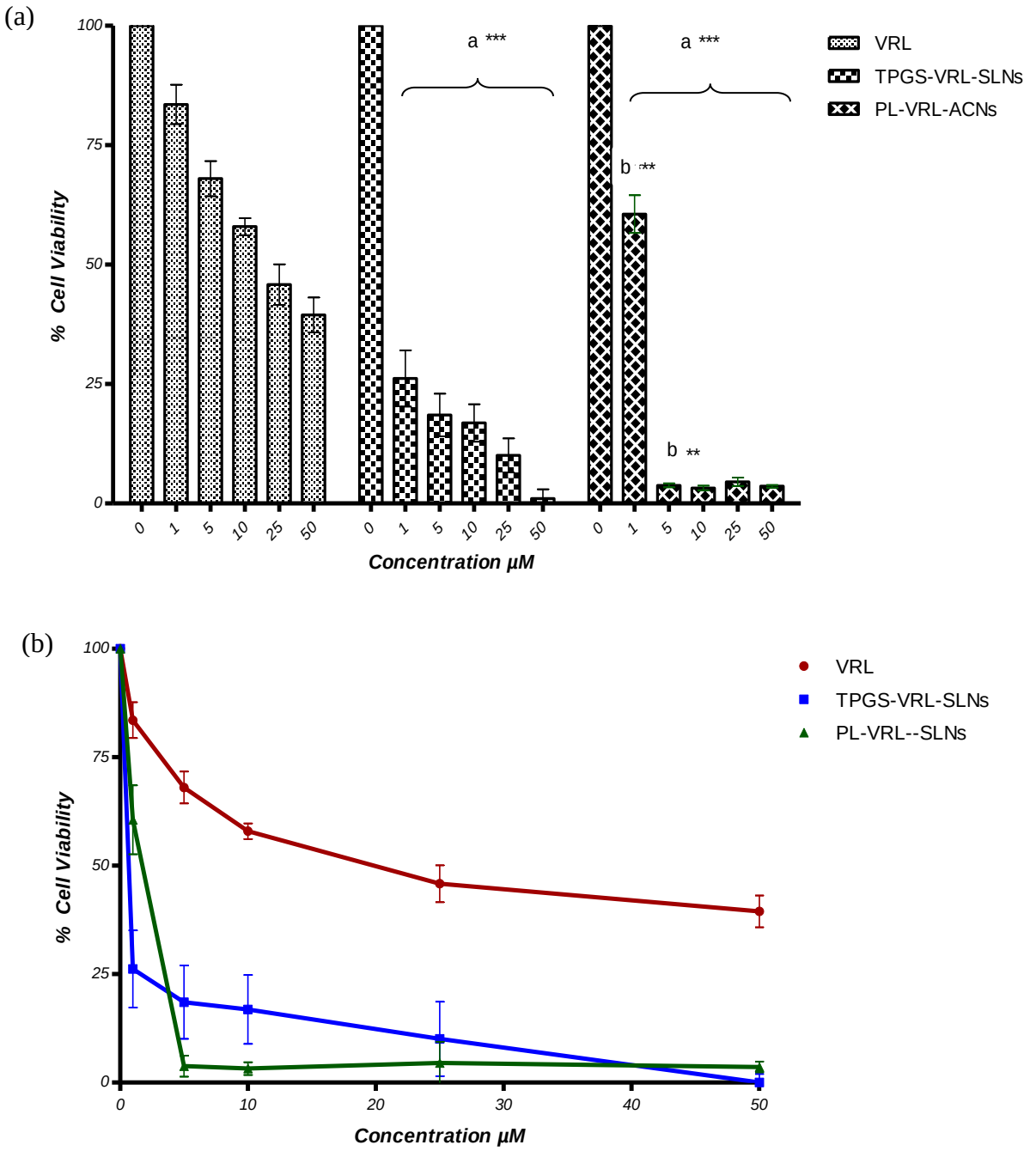

Figure 5.10: (a) Percentage cell viability of VRL, TPGS-VRL-SLNs and PL-VRL-SLNs at different concentrations. (b) Scatter plot for calculation of IC_{50}. Results were analyzed by two way ANOVA followed by bonferroni posthoc test ; a: when compared with VRL, b: when compared with TPGS-VRL-SLNs; (***p< 0.0001), (**p<0.001) and (*p<0.05))

5.3.5 Safety for intravenous administration

5.3.5.1 Haemolysis analysis

As the developed SLNs were meant for i.v administration, these formulations were evaluated for safety against intravenous administration. Haemolysis studies were performed with placebo-SLNs, TPGS-VRL-SLNs and PL-VRL-SLNs. An ideal *i.v.* formulation should not cause haemolysis and platelet aggregation and the spontaneous haemolysis limit should not be more than 10 % to preserve the integrity and functionality of erythrocytes in blood (Vijayakumar et al., 2016a, Vijayakumar et al., 2016b, Vijayakumar et al., 2016c). The results of our study suggested that the percentage haemolysis of VRL were in the recommended limits at all the concentrations up to 8h which suggested that the venous irritation associated with VRL is not accompanied by haemolysis . However, Placebo SLNs, TPGS-VRL-SLNs and PL-VRL-ACNs showed haemolysis limits which was above the acceptable limits. Hence the SLNs were not found to be suitable for intravenous administration.

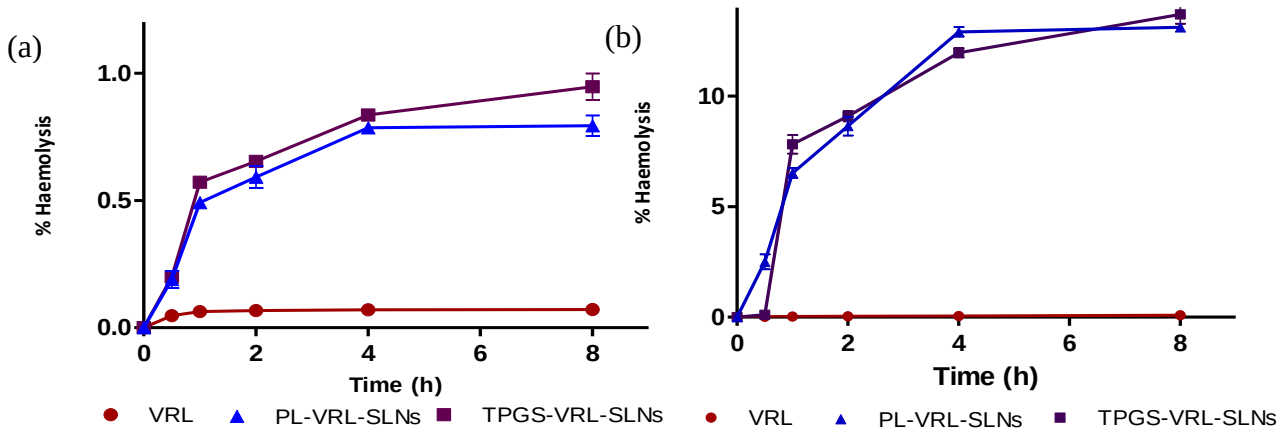

Figure 5.11: Percentage of haemolysis at different time intervals in whole blood samples after addition of test samples at (a) 10 and (b) 100 µg mL^{-1}

The TPGS-VRL-SLNs and PL-VRL-SLNs showed appreciable entrapment for water soluble VRL. The MTT assay further proved the higher cytotoxicity of both SLNs which can be attributed to the fusogenic nature of GMO. However, these SLNs were not suitable for intravenous administration hence further studies were not carried out on these formulations. Rather, it was decided to explore some other formulations which can overcome the drawbacks associated with GMO based SLNs.

5.4 Aqueous core nanocapsules (ACNs)

5.4.1 Experimental design

Box-behnken design (BBD) generated thirteen batches of GMS-VRL-ACNs using lipid concentration (X_1), surfactant concentration (X_2) and homogenization speed (X_3) as independent variables. The batches were prepared and analyzed for particle size and encapsulation efficiency (Table 5.10).The best model was selected based on R^2 value (should be close to 1), F value (should be high and p value (should be low) and polynomial equations were studied for the relationship of any variable on the measured response. The positive coefficient of any factor suggested direct relationship whereas the negative coefficient indicated inverse relationship. The 3D response surface plots were generated and the influences of independent variables on responses (particle size and encapsulation efficiency) were evaluated. Moreover, the influence of interactions among variables on response was also studied (Figure 5.12 and Figure 5.13:) (Mishra et al., 2017, Patel et al., 2016, Vardhan et al., 2017).

Table 5.10: Box Behnken design showing experimental runs with independent variables and their measured responses: particle size (nm) and encapsulation efficiency (%) of PLGA-VRL-ACNs and GMS-VRL-ACNs. Values are represented as mean ± S.D, n=3

Runs	**Independent variables**			**Dependent variables**			
				GMS-VRL-ACNs		**PLGA-VRL-ACNs**	
	X_1	X_2	X_3	P.S (nm)	EE (%)	P.S (nm)	EE (%)
1	15	0.4	5000	154.0 ± 3.1	45.0 ± 3.2	198.5 ± 3.4	64.2 ± 2.1
2	25	0.3	10000	210.0 ± 1.2	78.0 ± 2.1	143.2 ± 4.3	82.8 ± 4.1
3	25	0.4	5000	268.0 ± 1.2	54.0 ± 2.2	204 ± 4.2	79.8 ± 3.2
4	20	0.5	15000	154.0 ± 2.1	46.0 ± 2.1	106.7 ± 1.3	71.5 ± 2.1
5	20	0.3	15000	232.0 ± 1.1	75.0 ± 3.2	119.4 ± 2.1	74.78 ± 3.4
6	20	0.3	5000	287.0 ± 1.3	64.0 ± 2.1	199.5 ± 2.4	79.68 ± 2.2
7	15	0.5	10000	102.0 ± 2.1	45.0 ± 0.2	116.6 ± 3.2	65.2 ± 4.1
8	25	0.5	10000	187.0 ± 2.1	65.6 ± 1.2	116.6 ± 3.2	77.3 ± 2.1
9	20	0.5	5000	298.0 ± 1.1	64.0 ± 3.1	181.4 ± 4.3	77.7 ± 1.3
10	20	0.4	10000	182.0 ± 2.2	62.0 ± 3.1	120.8 ± 3.2	78.25 ± 2.1
11	25	0.4	15000	143.0 ± 1.2	66.2± 1.1	95.3 ± 3.2	77.98 ± 3.4
12	15	0.3	10000	120.0 ± 3.2	59.6 ± 2.1	133.6 ± 3.6	70.05 ± 2.2
13	15	0.4	15000	100.0 ± 2.3	35.0 ± 1.2	96.4 ± 2.1	70.4 ± 3.2

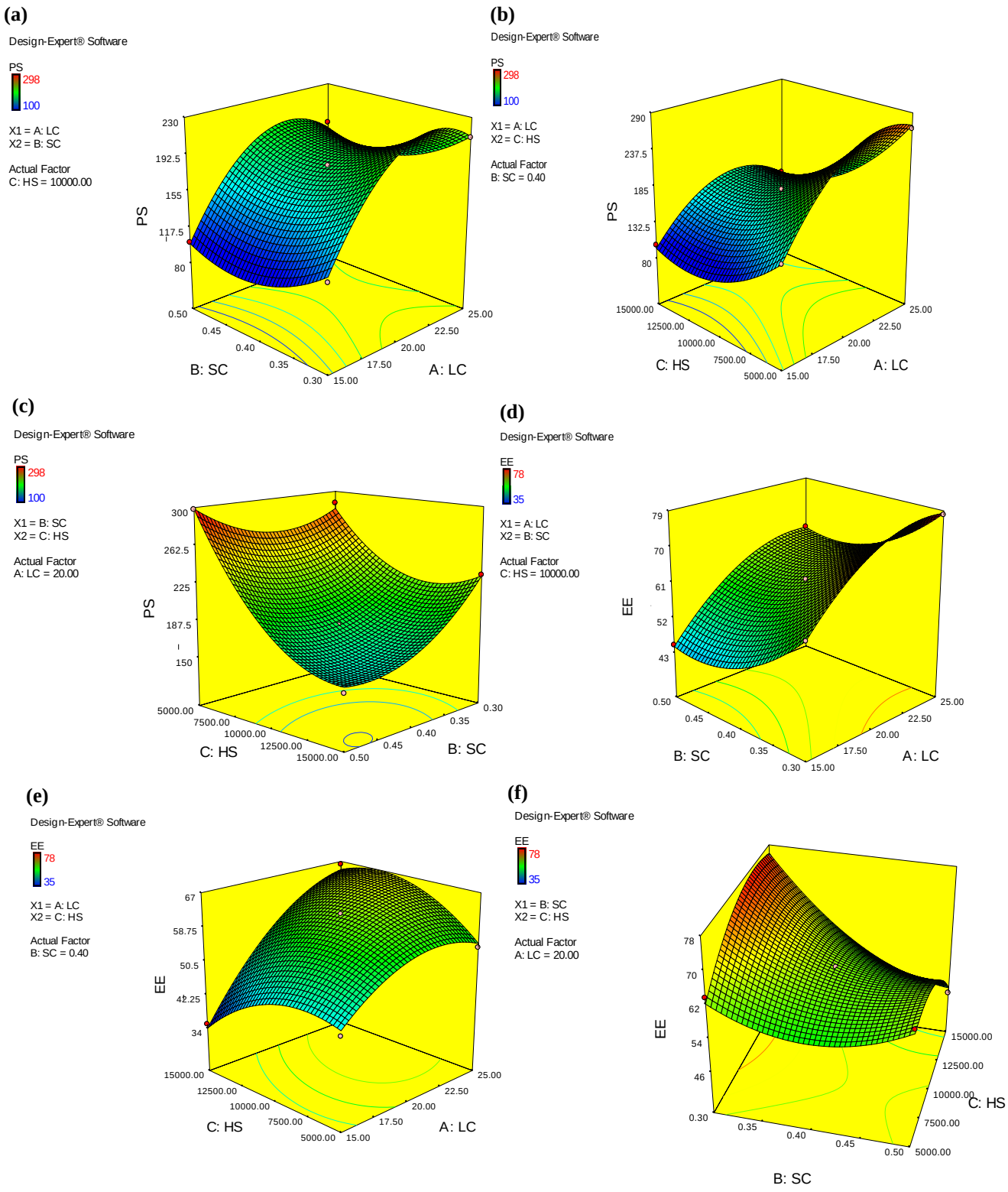

Figure 5.12: Three-dimensional response surface plots showing the effect of independent variables (LC: Lipid concentration, S.C: Surfactant concentration and H.S:homogenization speed) on response variables. P.S: Particle size (a, b, c) of GMS-VRL-ACNs; and EE: encapsulation efficiency (d, e, f) of GMS-VRL-ACNs

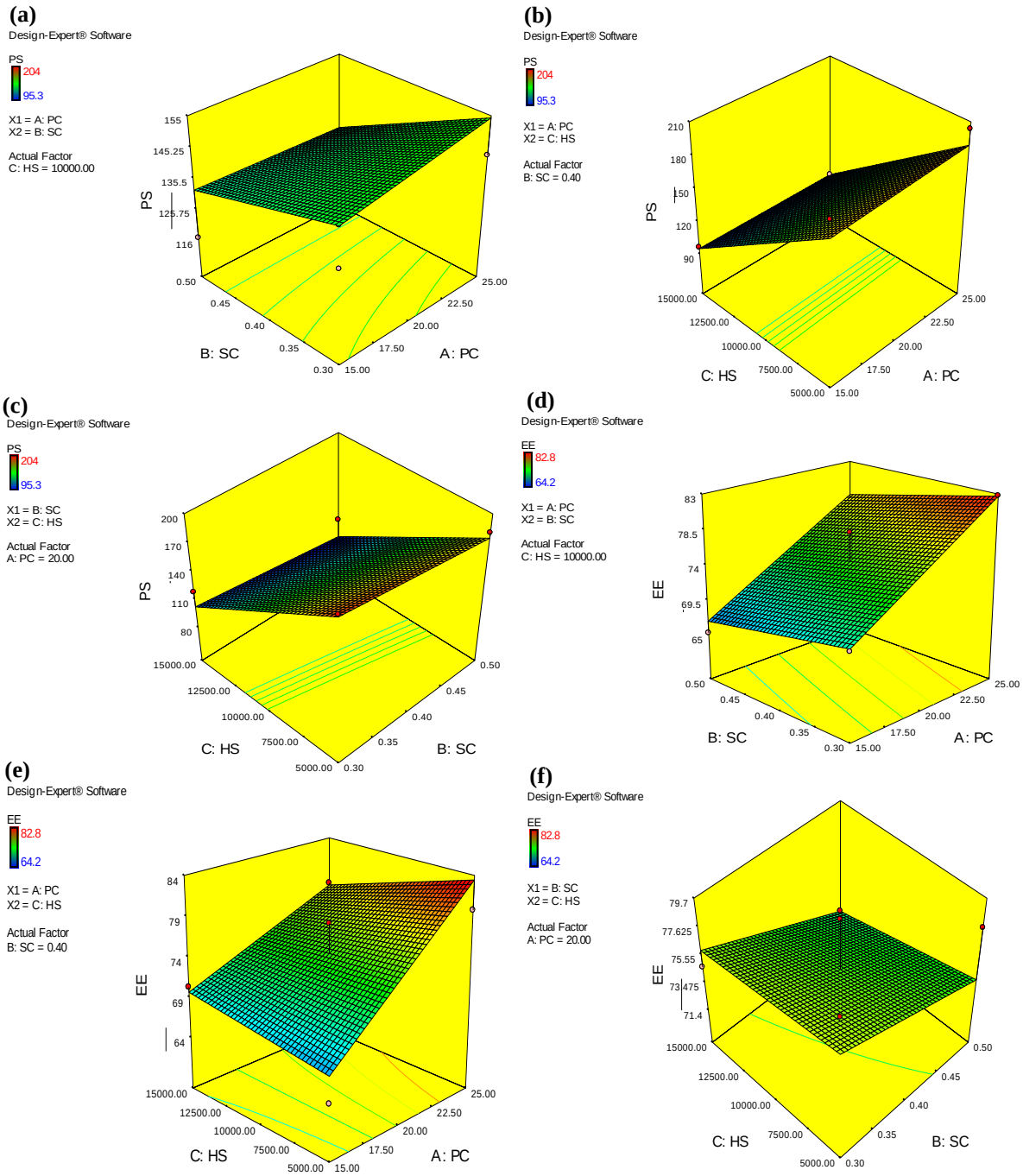

Figure 5.13: Three-dimensional response surface plots showing the effect of independent variables (PC: Lipid concentration, SC: Surfactant concentration and HS:homogenization speed) on response variables. P.S: Particle size (a, b, c) of PLGA-VRL-ACNs; and EE: encapsulation efficiency (d, e, f) of PLGA-VRL-ACNs

5.4.1.1 Influence of independent variables on particle size

GMS-VRL-ACNs and PLGA-VRL-ACNs were found to show particle sizes in the range of 100.0 ± 2.3nm to 298.0 ± 1.1 nm and 95.3 ± 3.2 nm to 204 ± 4.2 nm, respectively. The polynomial equations with constants and regression coefficients generated by multiple linear regressions for particle size for GMS-VRL-ACNs (Y_1) and PLGA-VRL-ACNs (Y_1^*) were given as:

$$Y_1 = 182 + 41.4\ X_1 – 13.5\ X_2 – 47.25\ X_3 - 1.25\ X_1X_2 – 17.75\ X_1X_3 – 22.25\ X_2X_3 – 51.88\ X_1^2 + 24.63\ X_2^2 + 36.12\ X_3^2$$ Equation 5.5

$$Y_2 = 140.92 + 1.75\ X_1 – 9.30\ X_2 – 45.70\ X_3 - 2.40\ X_1X_2 – 1.65\ X_1X_3 + 1.35\ X_2X_3$$ Equation 5.6

The quadratic model was found to best fit for analyzing the particle size of GMS-VRL-ACNs whereas linear model was best fitted for PLGA-VRL-ACNs. Both the models with high F value (104.15 and 22.88 for GMS-VRL-ACNs and PLGA-VRL-ACNs, respectively), lower p value (<0.0014 and <0.0002 for GMS-VRL-ACNs and PLGA-VRL-ACNs, respectively) and correlation coefficients close to one (i.e. R^2= 0.9968 and 0.8841 for GMS-VRL-ACNs and PLGA-VRL-ACNs, respectively) were found to be suitable for navigation of the design space(Joshi et al., 2010, Patel et al., 2016, Solanki et al., 2007) .

Though the amount of lipid and polymer used for the development of GMS-VRL-ACNs and PLGA-VRL-ACNs, respectively was very less, it affected the particle size non-significantly. A positive coefficient indicated direct relationship with particle size which can be attributed to the enhanced viscosity of the dispersed phase with increased lipid/polymer content. The viscosity reduced the stirring efficacy and hence droplet breakdown which eventually leads to higher particle size (Mishra et al., 2014, Patel et al., 2016). Surfactant concentration

negatively affected the particle size. The higher surfactant concentration leads to reduced interfacial tension between organic and aqueous phases which eventually forms smaller-sized droplets (Singh et al., 2014). The surfactant will further stabilize the droplets which results in small sized particles after evaporation of organic solvent (Mishra et al., 2014, Vuddanda et al., 2015). Homogenization speed also affects particle size negatively and the effect was found to be more pronounced. The nanocapsules were produced by double emulsion technique hence the development of small droplets is the most important step. The high intensity shear forces can overcome the resistance generated by viscosity, and intra-particle forces resulting in small particles (Anarjan et al., 2015, Kushwaha et al., 2013). These effects are further visualized clearly in 3D response surface graphs (Figure 5.12 and Figure 5.13:).

5.4.1.2 Influence of independent variables on encapsulation efficiency (EE)

GMS-VRL-ACNs and PLGA-VRL-ACNs showed encapsulation efficiency ranging from 35.0 ± 1.2 % to 78.0 ± 2.1 % and 64.2 ± 2.1 % to 82.2 ± 4.1 % , respectively, for various batches generated by BBD. The mathematical equation depicting the influence of independent variables on EE of GMS-VRL-ACNs (Y_1^*) and PLGA-VRL-ACNs (Y_2^*) can be given as follows:

$$Y_1^* = 62 + 9.90\ X_1 - 7.0\ X_2 - 0.6\ X_3 + 0.55\ X_1 X_2 + 5.55\ X_1 X_3 - 7.25\ X_2 X_3 - 6.07\ X_1^2 + 6.13\ X_2^2 - 5.88\ X_3^2$$ Equation 5.7

$$Y_2^* = 74.59 + 6.0\ X_1 - 1.96\ X_2 - 0.85\ X_3 - 0.18\ X_1 X_2 - 2.02\ X_1 X_3 - 0.32\ X_2 X_3$$ Equation 5.8

The respective models showed F, p and R^2 values of GMS-VRL-ACNs and PLGA-VRL-ACNs are given in

Table 5.11.

Table 5.11: Model parameters for optimization of GMS-VRL-ACNs and PL-VRL-ACNs

Formulation	Model	F	p	R^2
GMS-VRL-ACNs	Quadratic	56.78	< 0.0034	0.9942
PLGA-VRL-ACNs	Linear	11.98	< 0.0017	0.7997

The equations showed that the concentration of lipid or polymer directly affects the encapsulation efficiency. As more lipid/polymer is available for nanocapsules formation there are chances of deposition of more lipid as the shell which (Mishra et al., 2014) imparts diffusional barrier at the interface and restricts the outward movement of hydrophilic VRL towards the external aqueous environment, leading to an increase in EE (Patel et al., 2016). However, EE was found to decrease with the surfactant concentration which could be attributed to the reduced interfacial tension which ultimately enhances drug partitioning into the aqueous phase (Patel et al., 2016). Homogenization speed was found to have negligible effect on EE.

5.4.1.3 Determination of optimal conditions for the preparation of GMS-VRL-ACNs and PLGA-VRL-ACNs

Desirability approach was employed for numerical optimization. The optimized levels of independent variables for the preparation of ACNs with minimum particle size and maximum entrapment efficiency were predicted by applying the constraints. The optimized batches of GMS-VRL-ACNs and PLGA-VRL-ACNs were prepared with predictive levels and evaluated for the prediction error to validate the optimization process. The selected levels for the preparation of optimized batches of GMS-VRL-ACNs and PLGA-VRL-ACNs are shown in Table 5.12.

5.4.2 Characterization of GMS-VRL-ACNs

5.4.2.1 Particle size, PDI, encapsulation efficiency (EE) and zeta potential

The observed values of mean particle size, PDI and EE for the optimized batch of GMS-VRL-ACNs were found to be very close to the experimental values determined utilizing desirability approach. These values are shown in Table 5.12. The value of prediction error also suggested the predictability of the model (20, 21). The value of zeta potential for GMS-VRL–ACNs and PLGA-VRL-ACNs was found to be -15.6 ± 31 and -22.6 ± 2.1, respectively, indicating negative surface charges. The negative charge is imparted by the free carboxyl groups of TPGS (20) which have surface modifying properties (30). The protruding TPGS chains further provide steric hindrance and enhance the stability of GMS-VRL-ACNs and PLGA-VRL-ACNs.

Table 5.12: Optimized batch with measured responses using desirability approach by design expert

Variables	**Optimized value**			
	GMS-VRL-ACNs		**PLGA-VRL-ACNs**	
Polymer/Lipid concentration (X_1)	25		25	
Surfactant concentration (X_2)	0.34		0.3	
Homogenization speed (X_3)	13700		15000	
Results	**Predicted**	**Experimental**	**Predicted**	**Experimental**
Particle size (nm)	170.3	172.3 ± 2.1	105.6	110.3 ± 3.4
EE (%)	75.38	77.1 ± 2.3	80.2	82.1 ± 1.3
PDI	0.22 ± 0.20		0.12 ± 0.06	
Zeta Potential (mV)	-15.6 ± 3.1		-22.6 ± 2.1	

5.4.2.2 Transmission electron microscopy (TEM)

The TEM micrographs of GMS-VRL-ACNs are shown in Figure 5.14 which demonstrated the presence of smooth and spherical shaped ACNs. The particle size obtained by TEM correlated with that obtained by DLS. The figure depicted a central low dense aqueous core surrounded by dense lipidic shell. Moreover, the surface was covered by TPGS seen as loose layer surrounding nanocapsules. The diffraction pattern shows the crystallinity and amorphous nature of any sample. Here the figure shows diffused rings which suggested amorphous nature of the nanocapsules (Figure 5.15).

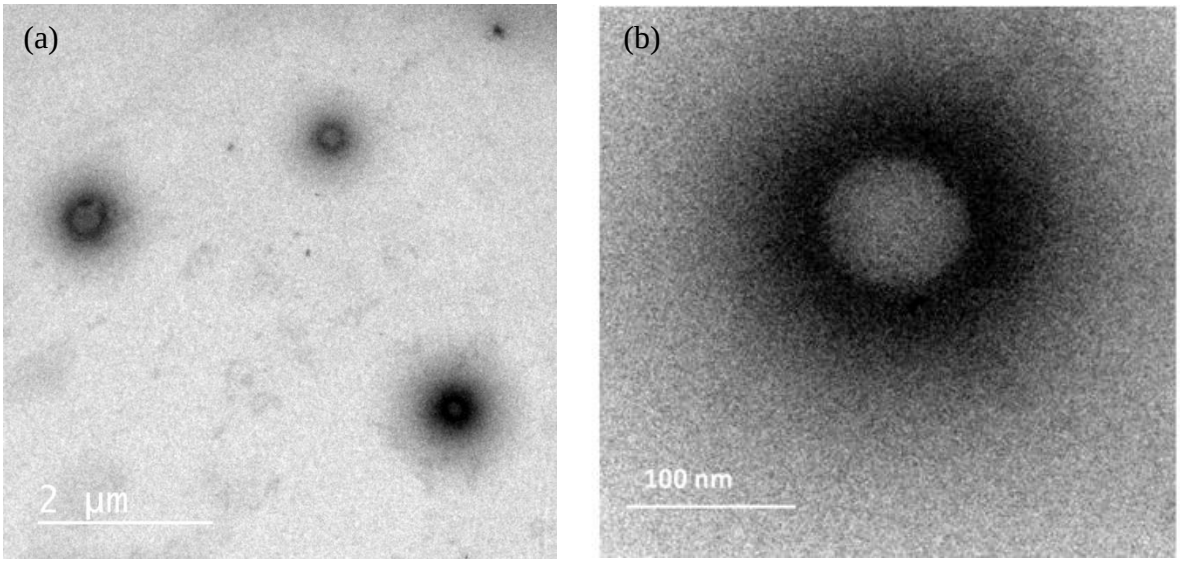

Figure 5.14: Surface morphology of (a) GMS-VRL-ACNs and (b) PLGA-VRL-ACNs by TEM

5.4.2.3 FTIR

The characteristic peaks of VRL were seen at 3250-3500 cm^{-1} (corresponds to N-H stretching) and 1750cm^{-1} (carbonyl group of ester).These characteristic peaks and peaks in

the finger print region correlated with the peaks obtained from physical mixture and lyophilized GMS-VRL-ACNs and PLGA-VRL-ACNs (Figure 5.16). Therefore, drug's identity was maintained during the preparation of nanocapsules.

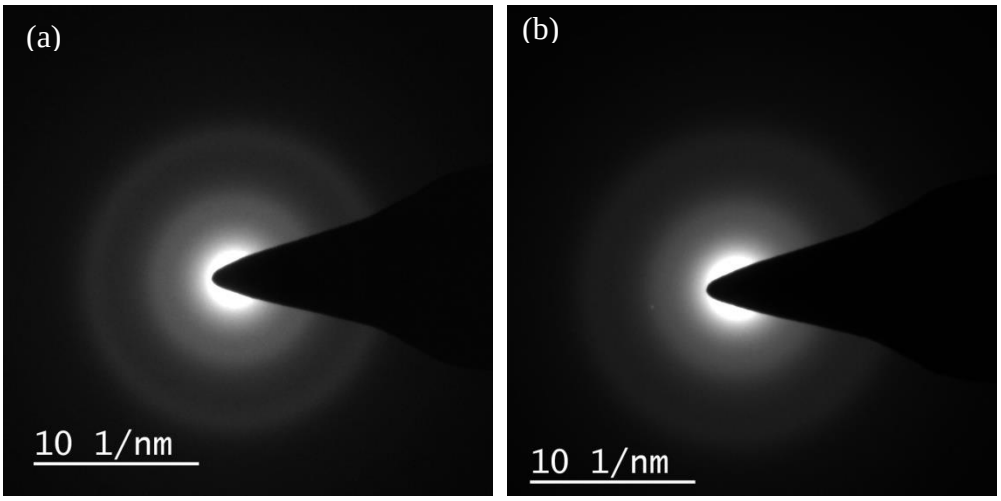

Figure 5.15: Diffraction pattern obtained by (a) GMS-VRL-ACNs and (b) PLGA-VRL-ACNs

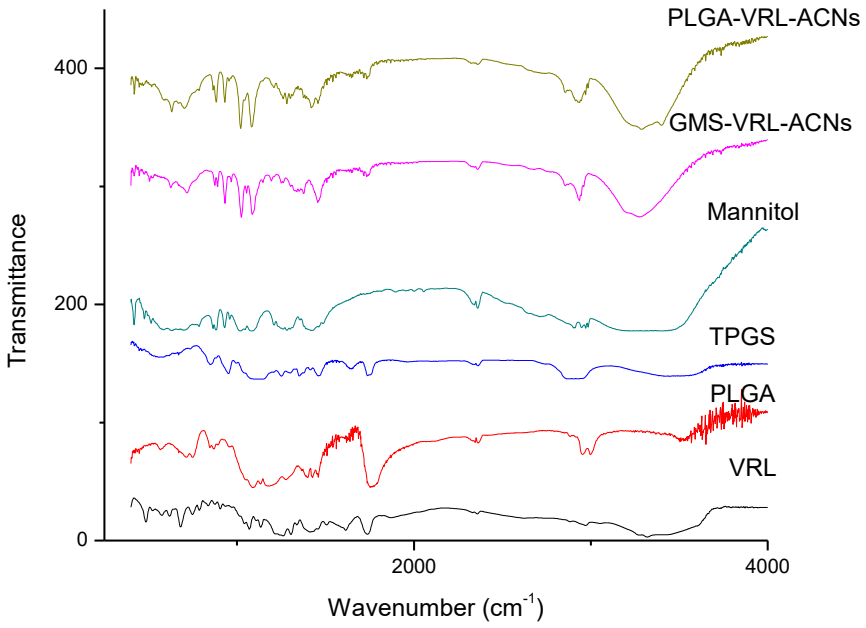

Figure 5.16: Drug excipient compatability studies by FTIR studies.

5.4.2.4 DSC

The DSC thermograms of VRL showed a broad endothermic peak in the temperature range of 180 to 220 ℃ corresponding to melting and a broad peak around 250 ℃ which corresponds to the degradation of VRL. The broad peaks suggested that VRL is more amorphous in nature .The physical mixture showed absence of melting peak and degradation peak which can be explained based on the high solubility of VRL in TPGS, a waxy surfactant. VRL as present in soluble form hence separate peaks were not observed. Similarly in lyophilized GMS-VRL-ACNs and PLGA-VRL-ACNs all peaks of VRL were absent.

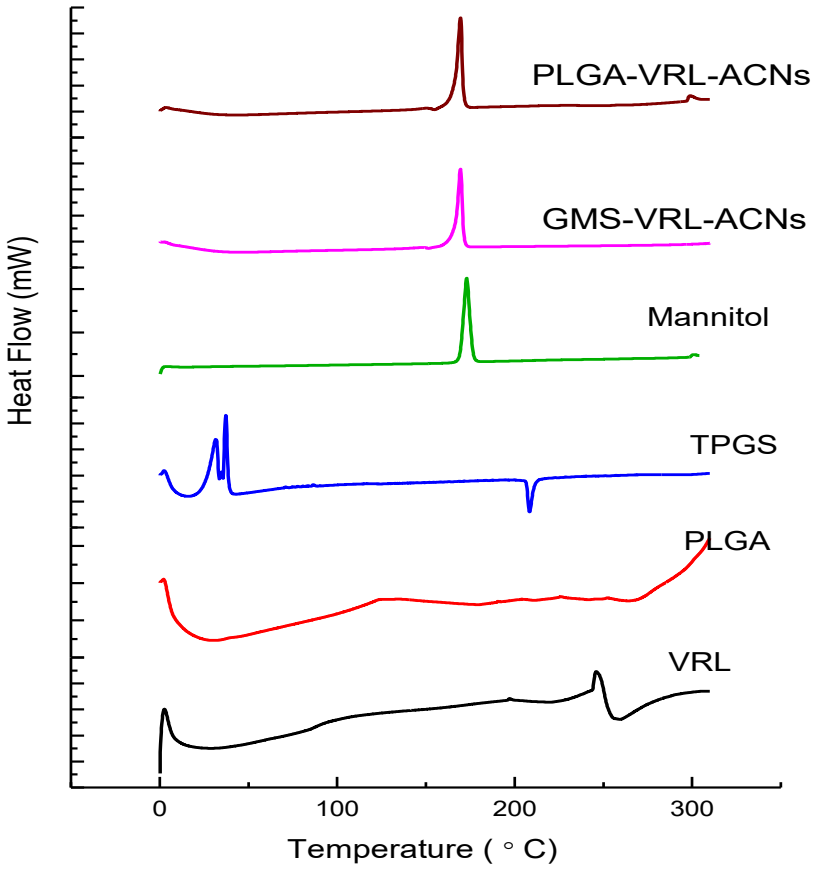

Figure 5.17: Drug excipient compatability studies by DSC studies. (a) GMS-VRL-ACNs and (b) PLGA-VRL-ACNs

The presence of a sharp peak nearly at 160 ^{o}C in lyophilized ACNs thermograrm is associated with the presence of mannitol which was used as a cryoprotectant during lyophillization of ACNs. The peaks of other excipients were also absent or reduced due to the solubility of all the ingredients in TPGS. The absence or reduction of peaks in DSC thermograms can be attributed to successful encapsulation of VRL into the GMS-VRL-ACNs.

5.4.2.5 In vitro drug release studies

The cumulative percentage release data (Figure 5.18) revealed sustained release of drug from GMS-VRL-ACNs. VRL solution showed more than 90% release in first 15 hours whereas the ACNs showed only 25 % release in the same duration. Moreover, in 24 hours VRL solution showed nearly 100 % release whereas GMS-VRL-ACNs leads to only 44 % release in 24 hours. Release from GMS-VRL-ACNs was found to be sustained as compared to pristine VRL. The initial burst release from ACNs might be due to the presence of some free drug in the nanosuspension and on the outer surface, the same can be supported by the encapsulation efficiency. The sustained release of VRL from ACNs can be attributed due to the presence of PLGA shell around the aqueous core which acts as a barrier for the release of VRL and the outer aqueous phase acts as driving force for the release of VRL. Moreover the release kinetics was found to follow Korsemeyer peppas model with $n < 0.5$, which suggested that the exact mechanism to be Fickian diffusion.

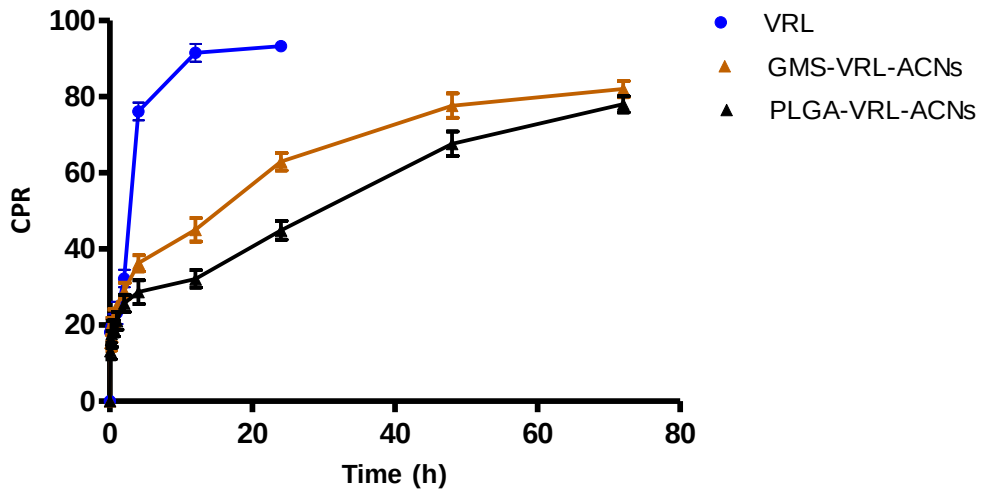

Figure 5.18: Cumulative Percentage Release (CPR) of drug from VRL solution, GMS-VRL-ACNs and PLGA-VRL-ACNs.

5.4.2.6 Stability studies

GMS-VRL-ACNs were found to be stable for 90 days without any significant change in the particle size, PDI and EE (Table 5.13).The value of zeta potential of the optimized batch was sufficient to stabilize the formulations. Moreover, the steric nature of TPGS further provides stability due to the presence of free carboxyl groups of TPGS over nanoparticle surface (20).

5.4.3 *In-vitro* cytotoxicity

MCF-7 cells in density of 1×10^4 cells per well were seeded in 96 well plates and incubated with different concentrations of PBS, VRL, Placebo-GMS-ACNs, Placebo-PLGA-ACNs, GMS-VRL-ACNs and PLGA-VRL-ACNs for 48 h. Placebo- ACNs were taken as positive control PBS as negative control during the study. Cell viability was determined with the help

of MTT assay and plotted against concentration (Figure 5.19) and the IC_{50} values for VRL, GMS-VRL-ACNs and PLGA-VRL-ACNs were determined. IC_{50} values of VRL, GMS-

Table 5.13: Particle size (nm) and Encapsulation efficiency (EE%) and Polydispersity Index (PDI) of PLG-VRL-ACNs at different time intervals at room temperature (30 ± 2 ℃/60 ± 5 % RH). Values are expressed as mean ± S.D (n=3).

Parameters	**Formulation**	**Days**			
		0	**30**	**60**	**90**
Particle size (nm)	GMS-VRL-ACNs	172.3 ± 2.1	182.3±2.2	195.3±3.3	201.3± 2.3
	PLGA-VRL-ACNs	110.3 ± 2.1	127.3 ± 2.2	134.3 ± 3.3	145.5 ± 1.3
PDI	GMS-VRL-ACNs	0.22 ± 0.20	0.37±0.02	0.43±0.02	0.43±0.02
	PLGA-VRL-ACNs	0.12 ± 0.06	0.37 ± 0.01	0.43 ± 0.02	0.44 ± 0.04
E.E (%)	GMS-VRL-ACNs	77.1 ± 2.3	75.6±2.5	68.3±3.1	62.3±3.0
	PLGA-VRL-ACNs	82.1 ± 2.3	79.6 ± 2.5	77.3 ± 3.0	75.6 ± 2.5

VRL-ACNs and PLGA-VRL-ACNs were found to be 19.75, 2.3 and 0.99 µM, respectively. The results of IC_{50} showed that the GMS-VRL-ACNs and PLGA-VRL-ACNs have 8.6 and 19.9 fold more inhibition compared to VRL. The additional cytotoxicity can be explained on the basis of cytotoxicity of the placebo formulation. The PLGA or GMS component in equivalent concentration was not found to predispose any cytotoxicity (data not shown) therefore, the anticancer activity of PLGA-VRL-ACNs and GMS-VRL-ACNs can be attributed to the presence of TPGS. The cytotoxic potential of TPGS has been already proved *in-vitro* and *in-vivo* for several types of cancer due to its P-gp inhibition potential (Mishra et al., 2017, Vijayakumar et al., 2016b).

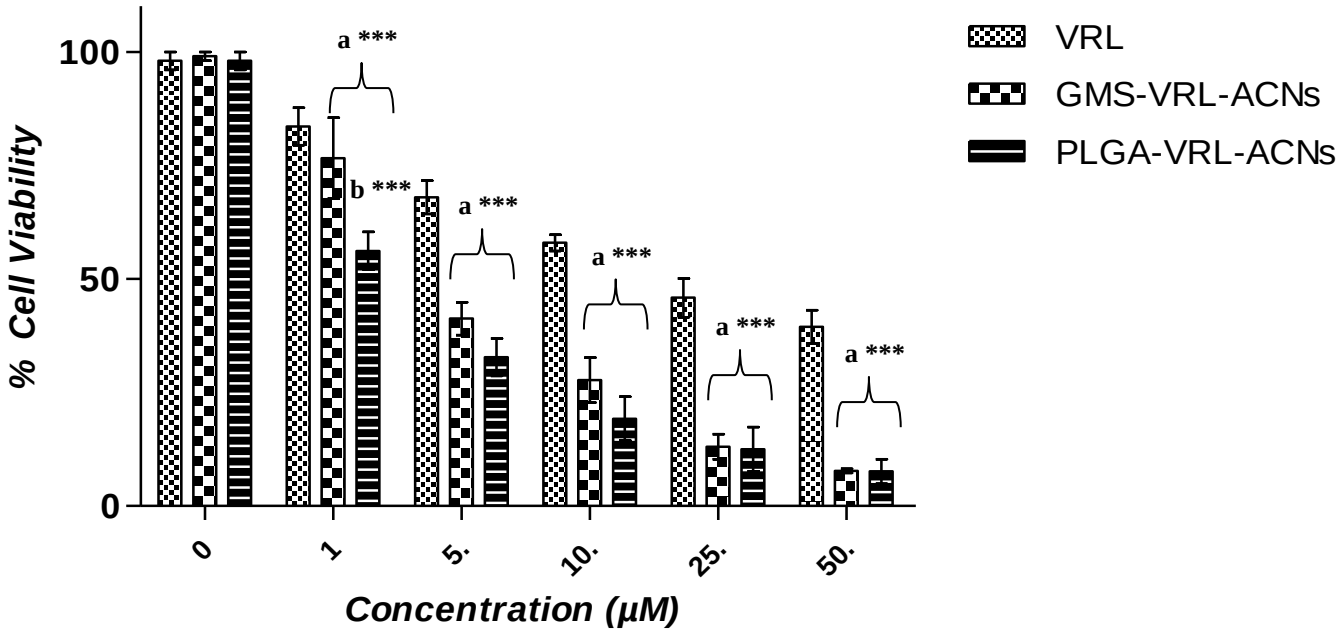

Figure 5.19: Cell viability of VRL, GMS-VRL-ACNs and PLGA-VRL-ACNs at different concentrations. (A) Results were analyzed by two way ANOVA followed by bonferroni posthoc test ; a: when compared with VRL, b: when compared with GMS-VRL-ACNs-ACNs; ((***p< 0.0001), (**p<0.001) and (*p<0.05))

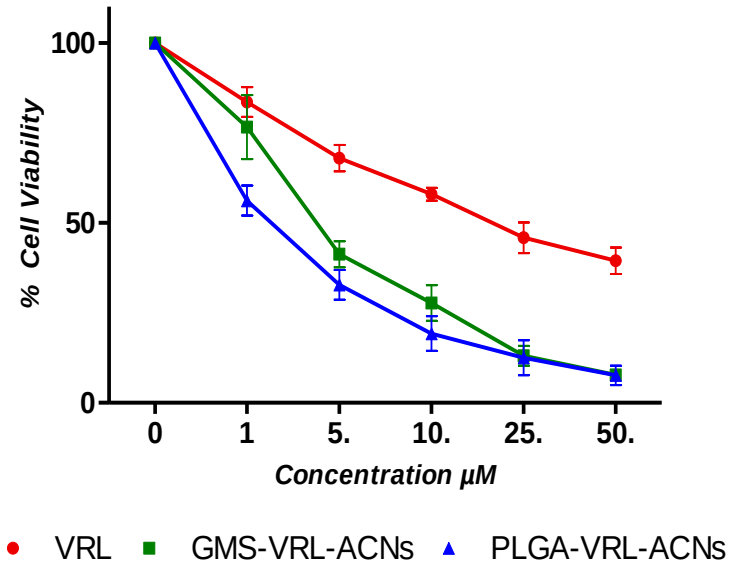

Figure 5.20: Scatter plot for determination of IC_{50}

5.4.4 Safety for intravenous administration

5.4.4.1 Haemolysis analysis

An ideal *i.v.* formulation should not cause haemolysis and platelet aggregation at the concentration intended for *i.v* administration. Spontaneous haemolysis limit should not be more than 1 % to preserve the integrity and functionality of erythrocytes in blood (Vijayakumar et al., 2016a, Vijayakumar et al., 2016b, Vijayakumar et al., 2016c). The results of our study suggested that the % haemolysis of VRL, Placebo ACN and GMS-VRL-ACNs were in the recommended limits at all the concentrations up to 8h (Figure 5.21).

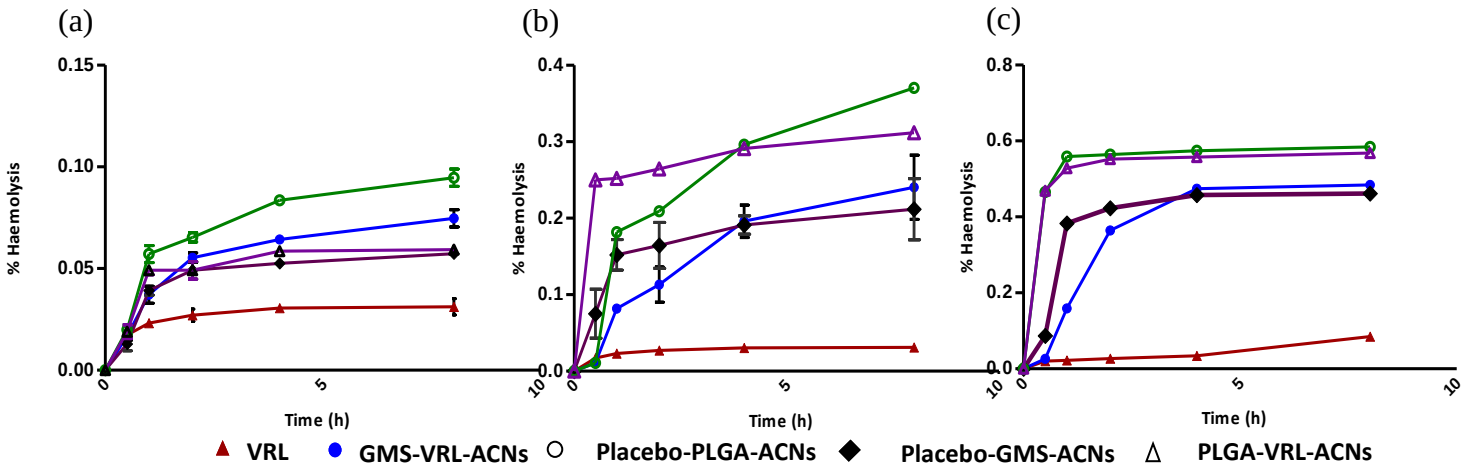

Figure 5.21: Percentage of haemolysis at different time intervals in whole blood samples after addition of VRL, placebo-ACNs, GMS-VRL-ACNs and PLGA-VRL-ACNs at (a) 10, (b) 50 and (c) 100 mg mL^{-1}. (d) Number of platelets after addition of PBS, VRL, placebo ACNs and PLGA-VRL-ACN at 10, 50 and 100 mg mL^{-1}. Values are represented as mean ± SD (n =3).

5.4.4.2 Platelet aggregation

As the developed GMS-VRL-ACNs were meant for *i.v* administration, the evaluation of platelet aggregation is essential. Platelet aggregation can cause thrombus formation and may precipitate various complications such as ischaemia, myocardial infarction or stroke. VRL doesn't causes platelet aggregation which can be clearly shown by the platelet counts of VRL-treated samples which were similar to platelet counts of PBS-treated samples at all the concentrations tested. Placebo-ACNs, GMS-VRL-ACNs and PLGA-VRL-ACNs showed platelet count similar to PBS-treated samples as shown in Figure 5.22.

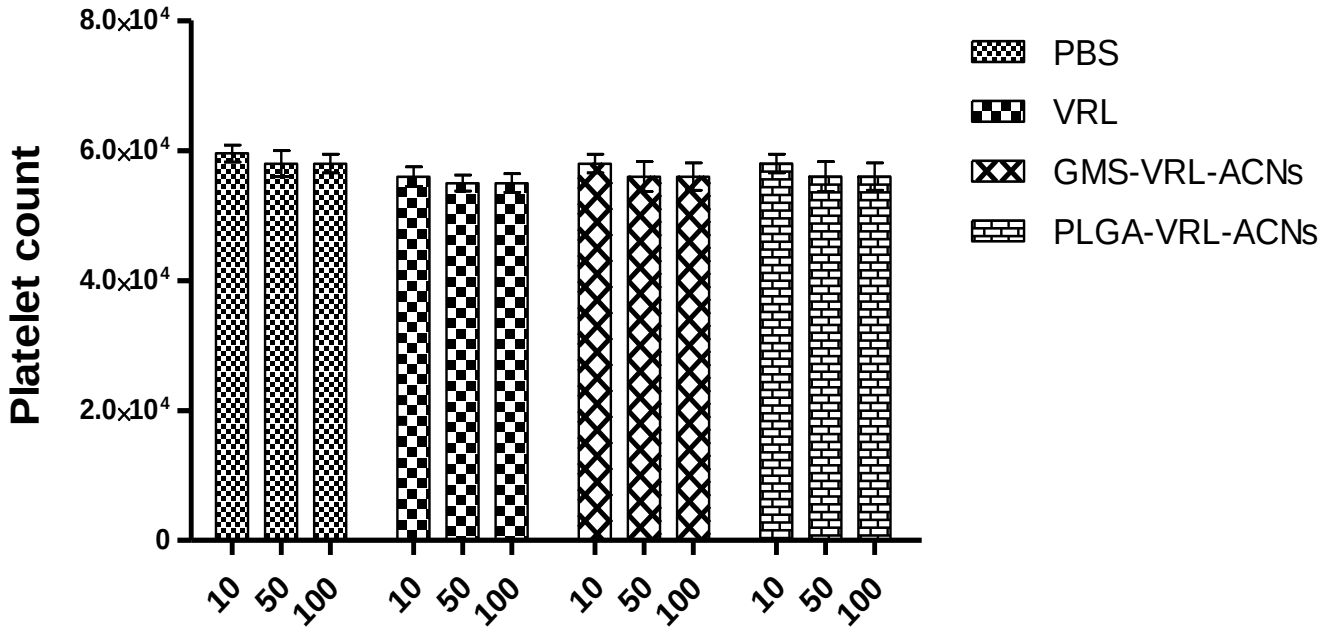

Figure 5.22: Number of platelets after addition of PBS, VRL, placebo ACNs, GMS-VRL-ACNs and PLGA-VRL-ACN at 10, 50 and 100 µg mL^{-1}. Values are represented as mean ± SD (n =3).

In addition to platelet count, the platelet aggregation in whole blood was observed by optical microscopy after incubation. Erythrocytes and platelets were visualized and the platelets are

indicated by arrow marks on the microphotographs (Figure 5.23). Supportively, no platelet aggregation was seen in all the samples at all the concentrations. All these observations indicated haemocompatibility of GMS-VRL-SLNs for the intravenous administration.

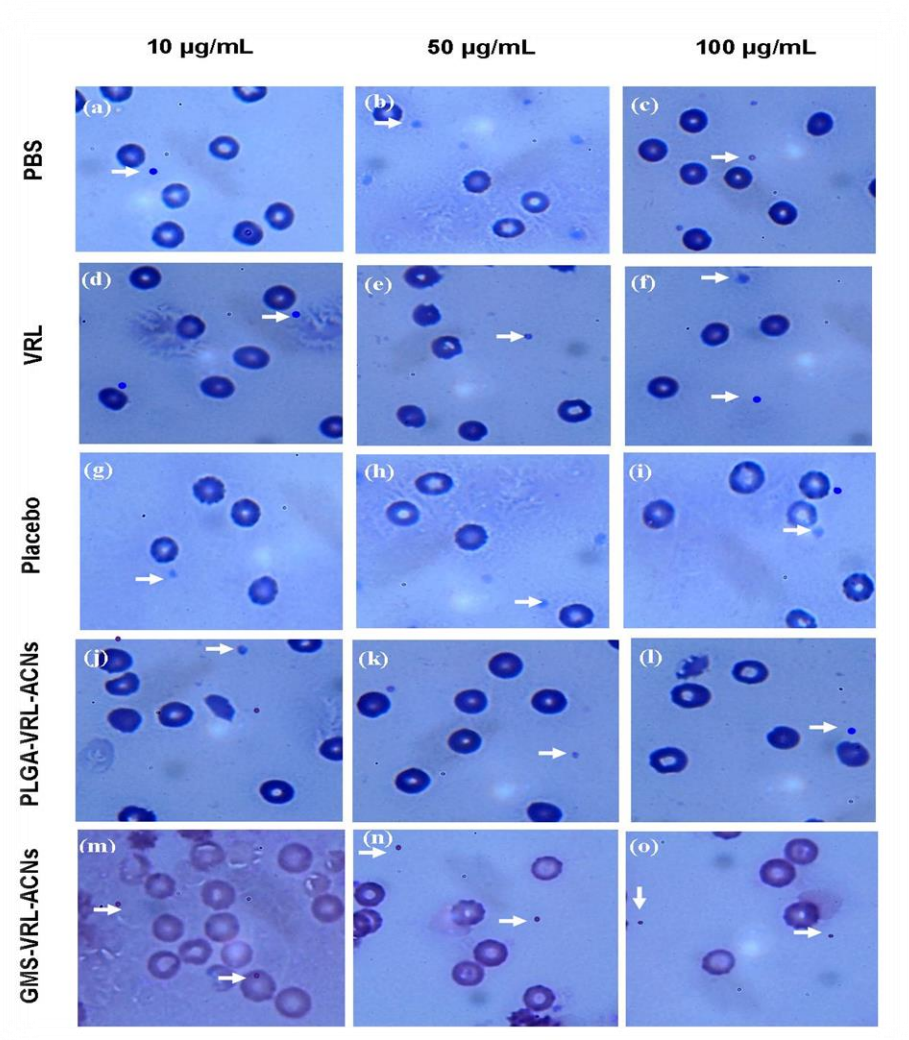

Figure 5.23: Qualitative platelet aggregation images of Leishman's stained whole blood samples after treatment with: (a) PBS (equivalent volume to 10, 50 and 100 µg mL^{-1} of test samples), (b) VRL (10, 50 and 100 µg mL^{-1}) and (c) PLGA-VRL-ACNs (10, 50 and 100 µg mL^{-1}). Images were captured at a magnification of 100×.

5.5 Dual drug loaded ACNs (dd-ACNs)

5.5.1 Determination of synergistic ratio of VRL and RES

5.5.1.1 Single drug treatment with VRL and RES

MCF-7 cell were seeded at a concentration of 1×10^4 and were treated with gradually increasing concentrations of VRL (0, 5, 10, 25 and 50 µM) for 24 h. Similarly treatment with RES was also given for 24 h. Figure 5.24 showed that the cell growth of MCF-7 cells was decreased VRL and RES both. These findings confirmed the cytotoxicity of VRL and RES as a single agent to inhibit MCF-7 cells. Further, studies were carried out to observe the the cytotoxicity of combination of drugs to study whether the combination is beneficial over either of the single drug.

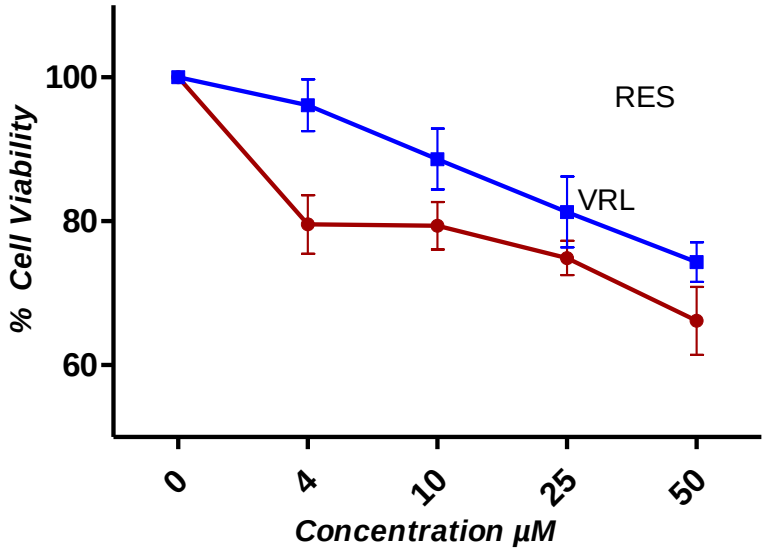

Figure 5.24: Single treatment with VRL and RES

5.5.1.2 Combination treatment with VRL and RES

The MTT assay was performed to study the effect of VRL and RES combination on cell viability. MCF-7 cell line was treated with VRL (0, 5, 10, 25 and 50 µM), RES (0, 5, 10, 25 and 50 µM), or VRL plus RES for 48 h and cell viability was evaluated (Wang et al., 2014). Treatment of MCF-7 cells with VRL plus RES for 48 h resulted in significant decrease in cell viability which was greater than either VRL or RES alone Figure 5.24. Fraction affected (Fa) were obtained after exposure of the MCF-7 cells to a series of drug concentrations. To study the effects at different Fa values, CI (combination index) and DRI (dose reduction index) values were calculated for each Fa. Figure 5.25 shows the Fa-CI plots depicting the effects of VRL and RES at different constant drug ratios which displayed synergism (CI<1) at Fa>0.6. The data reported CI < 1 and DRI > 1 for 1:10, 1:1, 5:1 and 10:1. However, 1:5 resulted in antagonistic combination with CI >1 and DRI <1. Generally, synergism corresponding to CI<1 always yielded a favorable DRI >1 for both drugs. The Fa-DRI plots are shown in Figure 5.25, and indicated that chemotherapeutic doses of VRL may be significantly reduced for combinations with RES that are synergistic at Fa.0.6. Classical isobolograms at IC_{75} (Figure 5.25 (c)) also indicates synergism where we can see that (cVRL, cRES) is located below the line of synergy for all ratios except 1:5. As synergism was observed at higher VRL proportions, the 10:1 ratio showing maximum synergy was selected for the preparation of nanocapsules.

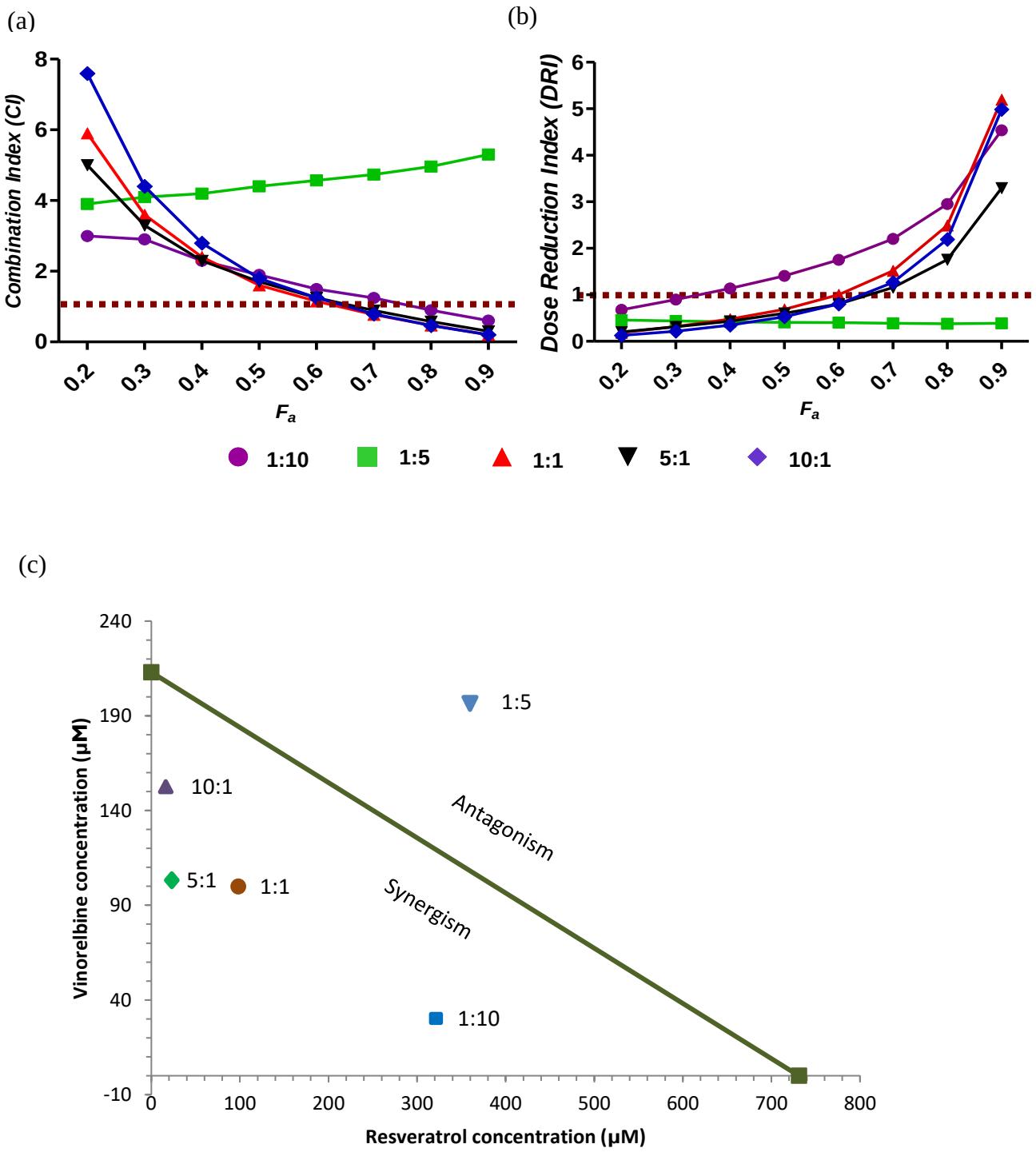

Figure 5.25:Illustrative Fa-CI and Fa-DRI plots for the combination of VRL and RES using different fixed drug ratios. (a) CI values were calculated from each Fa for MCF-7 cell lines. (b) DRI values were calculated from each Fa for MCF-7 cells. (c) Classical isobologram at IC_{75}

5.5.2 Characterization of ACNs

5.5.2.1 Particle size, PDI, and encapsulation efficiency

The mean particle size, PDI and EE of the optimized batch of GMS-VRL-RES-ACNs and PLGA-VRL-RES-ACNs were shown in Table 5.14. The PLGA based nanocapsules were found to have less particle size as compared to Lipid based dd-ACNs

Table 5.14: Particle size, Zeta potential and PDI of GMS-VRL-RES-ACNs and PLGA-VRL-RES-ACNs. All results are presented as mean ± SD; n=3.

Formulation	**Particle size (nm)**	**Zeta potential (mV)**	**PDI**
GMS-VRL-RES-ACNs	160.3 ± 4.23	-19.6 ± 2.1	0.12 ± 0.06
PLGA-VRL-RES-ACNs	150.2 ± 3.2	-18.12 ± 0.2	0.321± 0.02

5.5.2.2 Zeta potential

Zeta potential is defined by surface charge and high absolute values are associated with the stability of the colloidal dispersions which in turn is affected by the chemical structure of the molecules involved in the formulation. The value of zeta potential for GMS-VRL-RES-ACNs and PLGA-VRL-RES-ACNs was found to be -19.6 ± 2.1 and -18.12 ± 0.2 indicating negative surface charge. Negative charge can be attributed to presence of PLGA/GMS involved in the formulation of dd-ACNs and free carboxyl groups of TPGS which is already proven for its surface modifying properties. In surface modification a tiny steric layer was formed on surface of core particle which prevents agglomeration even at neutral zeta potential region. The protruding TPGS chains hence enhance the stability of the PLGA-VRL-

ACNs by providing steric hindrance (Kulkarni and Feng, 2013, Mishra et al., 2017, Vijayakumar et al., 2016b, Vuddanda et al., 2014, Wang et al., 2013).

5.5.2.3 Transmission electron microscopy (TEM)

GMS-VRL-RES-ACNs and PLGA-VRL-RES-ACNs were found to be spherical in shape with smooth surface. Figure 5.26 clearly depicted a central low dense cavity corresponding to aqueous core surrounded by dense solid layer which corresponds to polymeric shell. The presence of two cavities was further confirmed by the diffraction analysis (data not shown). A diffuse layer was also seen over the surface of nanocapsules which corresponds to TPGS which is already been proved for surface modifying properties (Vuddanda et al., 2014).

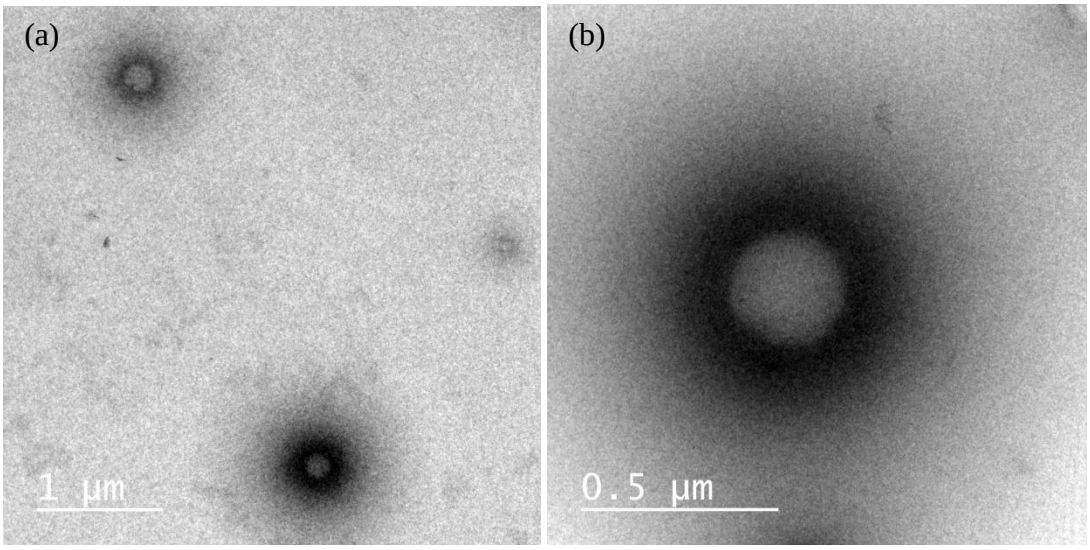

Figure 5.26: Surface morphology of (a) GMS-VRL-RES-ACNs and (b) PLGA-VRL-RES-ACNs by Transmission electron microscopy (TEM)

5.5.2.4 FTIR

VRL formed its characteristic band near 3250-3500 cm^{-1} (corresponds to N-H stretching), 1750cm^{-1} (carbonyl group of ester) whereas RES showed characteristics peaks at 3288.7 cm-1 (O-H streching), 1606.7 (C=C stretching for olefinic group), 1587.4 & 1442.8 (C=C stretching for aromatic group), 1153.4 (C-O stretching) and 964.4 (trans olefinic bond). The peaks of VRL and RES were well correlated with the peaks obtained from lyophilized dd-ACNs (Figure 5.27). Therefore, there was absence of any physical and chemical changes in the drug's identity during preparation of nanocapsules.

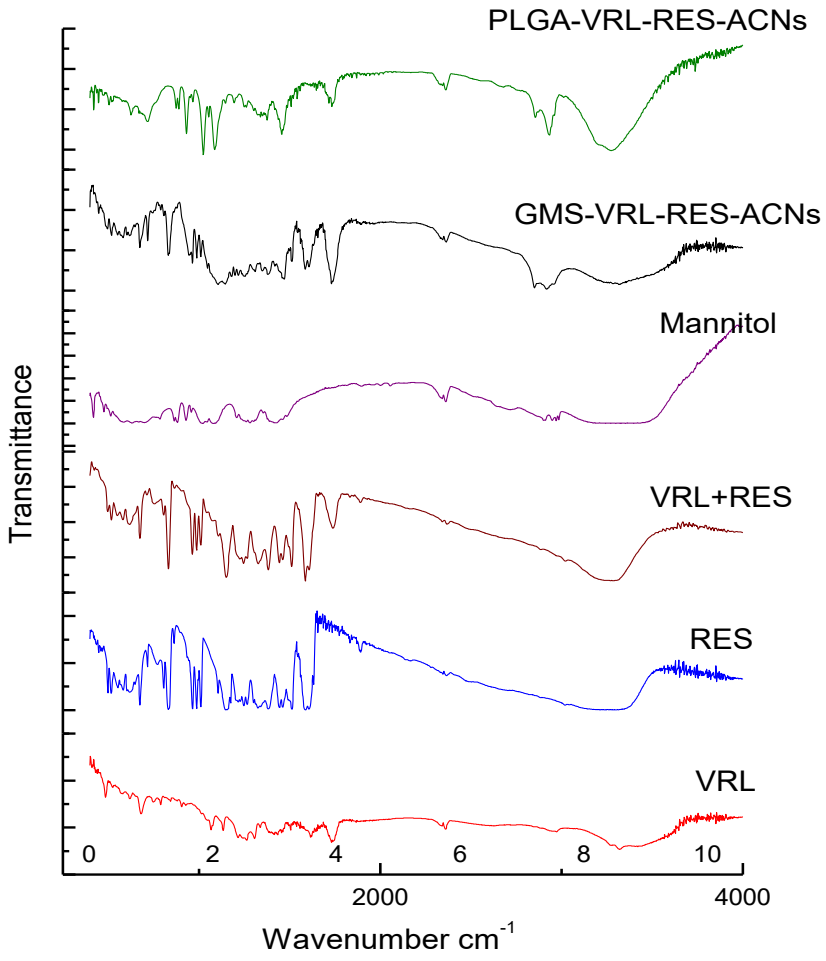

Figure 5.27: Drug excipient compatibility by FTIR

5.5.2.5 DSC analysis

The DSC thermograms (Figure 5.28of VRL showed broad endothermic peaks in the temperature range of 100 - 160 ℃ and 190 – 220 ℃. An exothermic peak was also observed nearly 250 ℃. The reduced intensity of these peaks suggested absence of any obvious melting point for VRL hence non-crystalline nature of VRL. RSV was found to show a peak at 267.71 ℃. The thermograms of dd-ACNs displayed the individual peaks of VRL in their original shape with reduction in intensity which can be attributed to encapsulation of VRL in the PLGA matrix of ACNs. The presence of peaks in ACNs also suggested absence of any interaction among excipients. The absence of RSV peak suggested marked encapsulation of RSV in dd-ACNs.

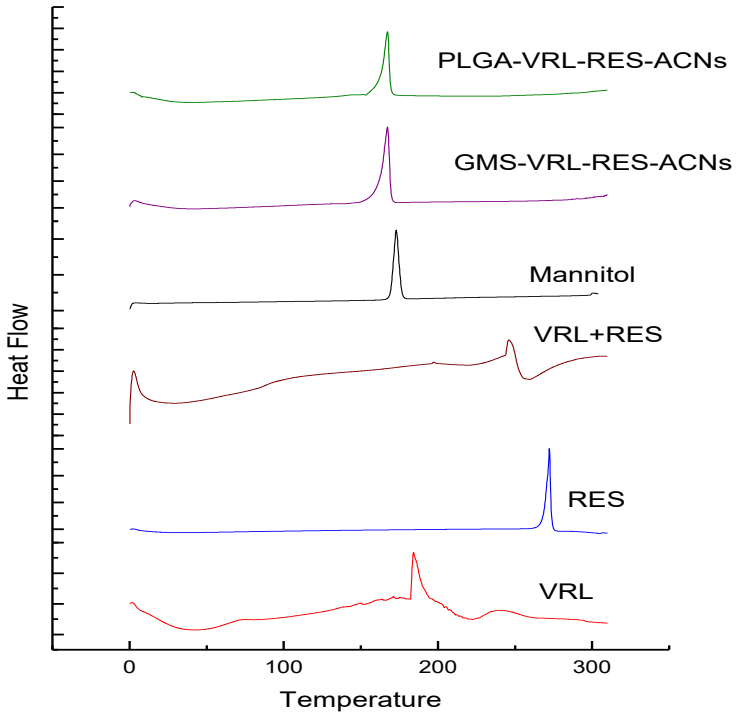

Figure 5.28: Drug excipient compatibility by DSC analysis

5.5.2.6 In-vitro drug release studies

The cumulative percentage release data (Figure 5.29) revealed sustained release of VRL and RES from dd-ACNs. VRL was released more rapidly than RES from dd-ACNs which is due to high solubility of VRL compared to RES. The release kinetics was found to follow Korsemeyer peppas model with n value of < 0.5, which suggested that the mechanism of drug release to be fickian diffusion for both drugs. Although both drugs were released at different rates, the dd-ACNs were able to maintain a synergistic drug ratio between 1:1 and 10:1. These results demonstrated that both the dd-ACNs released VRL and RES in a controlled manner which facilitated the delivery of therapeutic agents to the tumor site at their optimal synergistic ratio.

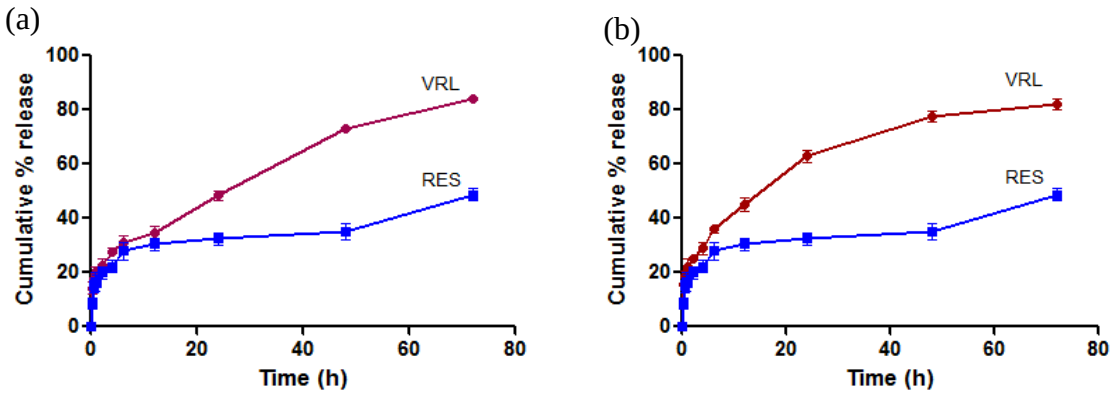

Figure 5.29: Cumulative percentage drug release of (A) GMS-VRL-RES-ACNs and (B) PLGA-VRL-RES-ACNs in PBS, pH 7.4 plus 5 % tween 80

5.5.2.7 Stability studies

Both dd-ACNs were found to be stable for 90 days without any significant change in the particle size, PDI and EE (Table 5.15). The value of zeta potential of the optimized batch was sufficient to stabilize the formulations. Moreover, the steric nature of TPGS (Kulkarni and

Feng, 2013, Vuddanda et al., 2014) further provide stability due to presence of free carboxyl groups of TPGS over nanoparticle surface.

Table 5.15: Particle size (nm) and Encapsulation efficiency (EE%) and Polydispersity Index (PDI) of PLGA-VRL-RES-ACNs and GMS-VRL-RES-ACNs at different time intervals at room temperature (30±2 °C/60±5 % RH). Values are represented as mean ± SD (n=3).

Formulation	**Parameters**	**Days**			
		0	**30**	**60**	**90**
GMS-VRL-RES-ACNs	**Particle size (nm)**	160.3 ± 4.23	172.2 ± 3.21	160.3 ± 4.23	172.2 ± 3.21
	PDI	0.12 ± 0.06	0.21 ± 0.12	0.23 ± 0.16	0.34 ± 0.12
	E.E (%)VRL	81 ± 2.34	77.6 ± 3.2	67.8 ± 5.4	63.46 ± 4.2
	EE (%)RES	98.6 ± 1.12	94.5 ± 2.12	72.6 ± 3.12	69.5 ± 5.25
PLGA-VRL-RES-ACNs	**Particle size (nm)**	150.2 ± 3.2	162.3 ± 3.2	175.3 ± 2.3	180.5 ± 2.3
	PDI	0.321± 0.02	0.27 ± 0.01	0.42 ± 0.02	0.41 ± 0.02
	E.E (%)VRL	80 ± 3.23	78.3 ± 3.5	75.4 ± 4.5	73.4 ± 3.5
	EE (%)RES	99.3 ± 1.21	95.4± 2.5	91.5± 4.5	87.4± 3.5

.

5.5.3 Cytotoxicity Studies against MCF-7 breast cancer cell line

MCF-7 cells in density of 1×10^4 cells per well were seeded in 96 well plates and incubated with different concentrations of VRL, VRL+RES, GMS-VRL-RES-ACNs and PLGA-VRL-RES-ACNs for 48 h. Placebo dd-ACNs were taken as positive control and PBS as negative control during the study. Cell viability was determined with the help of MTT assay and the results showed that the PLGA-VRL-ACNs and PLGA-VRL-RES-ACNs showed more inhibition compared to free drug and drug combination. Initially the cell viability was found

to be enhanced with combination of VRL and RES which can be explained on the basis of proliferative activity of RES. However, combination showed reduction in the IC_{50} several folds for dd-ACNs and GMS-VRL-RES-ACNs and PLGA-VRL-RES-ACNs were found to be 16-fold and 32-fold more effective compared to free VRL. The enhanced anticancer activity of can be attributed to the enhanced permeability of as well as presence of TPGS which has been proved to possess anticancer activity by inhibiting efflux of drugs from the cancer cells (Mishra et al., 2017, Vijayakumar et al., 2016b). Further, the synergistic combination loaded nanocapsules showed significantly high cytotoxicity compared to single drug loaded nanocaplues which can be attributed to delivery of synergistic combination to MCF-7 cells (Ashley et al., 2016).

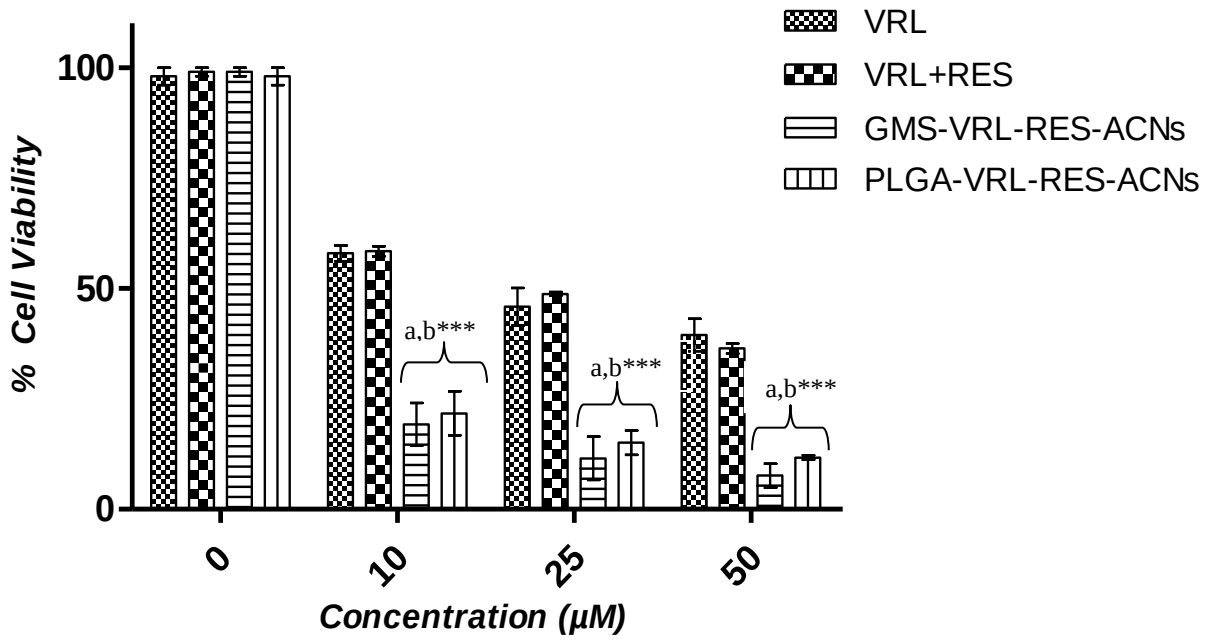

Figure 5.30: In vitro cytotoxicity of different formulations. Results were analyzed by two way ANOVA followed by bonferroni posthoc test ; a: when compared with VRL; b: when compared to VRL+RES; c: when compared to GMS-VRL-RES-ACNs; ((***p< 0.0001), (**p<0.001) and (*p<0.05))

5.6 Comparative study of all formulations

Table 5.16 summarizes the results of *in-vitro* analyses of all the developed nanocarriers. The results suggested that all nanoformulations showed optimum particle size, entrapment efficiency and sustained release for chemotherapeutic efficacy. All nanoformulations showed higher *in-vitro* cytotoxicity compared to pristine VRL. Although TPGS-VRL-SLNs showed the highest cytotoxicity among developed formulations but depicts lower entrapment compared to ACNs. Moreover, the haemolytic potential of GMO formulations restricted their testing in animals. All other formulations i.e. GMS-VRL-ACNs, PLGA-VRL-ACNs, GMS-VRL-RES-ACNs and PLGA-VRL-RES-ACNs were found to be haemocompatible and showed nearly 8, 20, 16 and 32 folds higher cytotoxicity, respectively, compared to pristine VRL. Hence, PLGA-VRL-RES-ACNs were selected for *in-vivo* studies and tested for systemic toxicity and *in-vivo* anticancer efficacy in 4T1 tumor grafted Balb/c mice model.

Table 5.16: Comparative results of TPGS-VRL-SLNs, PL-VRL-SLNs, GMS-VRL-ACNs and PLGA-VRL-ACNs

Paramaters	**VRL-SLNs**		**VRL-ACNs**		**dd-ACNs**	
	TPGS-VRL-SLNs	**PL-VRL-SLNs**	**GMS-VRL-ACNs**	**PLGA-VRL-ACNs**	**GMS-VRL-RES-ACNs**	**PLGA-VRL-RES-ACNs**
Particle Size (nm)	249.4 ± 8.1	234.6 ± 9.2	172.3 ± 2.1	110.3 ± 3.4	160.3 ± 4.23	150.2 ± 3.2
PDI	0.23 ± 0.1	0.310 ± 0.1	0.22 ± 0.20	0.12 ± 0.06	0.12 ± 0.06	0.321± 0.02
Zeta potential (mV)	-10.6 ± 2.1	-11.02 ± 0.4	-15.6 ± 3.1	-22.6 ± 2.1	-19.6 ± 2.1	-18.12 ± 0.2
Shape	Spherical matrix systems		Core shell structure			
Entrapment efficiency (%)	55.3 ± 2.3	58.45 ± 2.1	77.1 ± 2.3	82.1 ± 1.3	81 ± 2.34 (VRL) 98.6 ± 1.12 (RES)	80 ± 3.23 (VRL) 99.3 ± 1.21 (RES)
In-vitro release	Korsemeyer peppas model, n < 0.5		Korsemeyer peppas model, n < 0.5			
Interaction analysis	No potential chemical interactions found					
Cytotoxicity (In comparison to VRL)	Higher 39.5 fold	Higher 11.28 fold	Higher 8.6 fold	Higher 19.9 folds	Higher 16 fold	Higher 32 folds
Haemocompatibility	>1% Haemolysis limit suggested not safe for i.v. administration		< 1% Haemolysis limit suggested safety for i.v. administration		--	--

5.6.1 *In-vivo* studies

5.6.1.1 Toxicity studies

Figure 5.31 shows the changes in various biochemical parameters in the serum of rats treated with PBS, VRL, VRL+RES and PLGA-VRL-RES-ACNs. VRL increased the level of ALP, AST and TBIL and decreased the level of ALT which proved marked liver damage. However VRL+RES showed levels which were close to that of control group which can be explained on the basis of hepatoprotective nature of RES (De La Lastra and Villegas, 2007). PLGA-VRL-ACNs were found to elevate the serum biomarkers during initial days of studies which were found to normalize with time up to 28 days wherever PLGA-VRL-RES-ACNs showed levels which differ non-significantly from control. These results suggests that incorporation of RES with free drug in nanocapsules significantly reduced the systemic toxicity of VRL owing to hepatoprotective nature of RES. Similarly, VRL resulted in increased urea. However the dd-ACNs resulted in urea levels similar to control. Some studies reported nephrotoxicity associated with RES however the concentration used were such which didn't precipitate any potential nephrotoxicity. Other markers were not different between the groups. The results suggest that PLGA-VRL-RES-ACNs were non toxic after intravenous administration and RES can protect tissues from the toxic effects of VRL *in-vivo.*

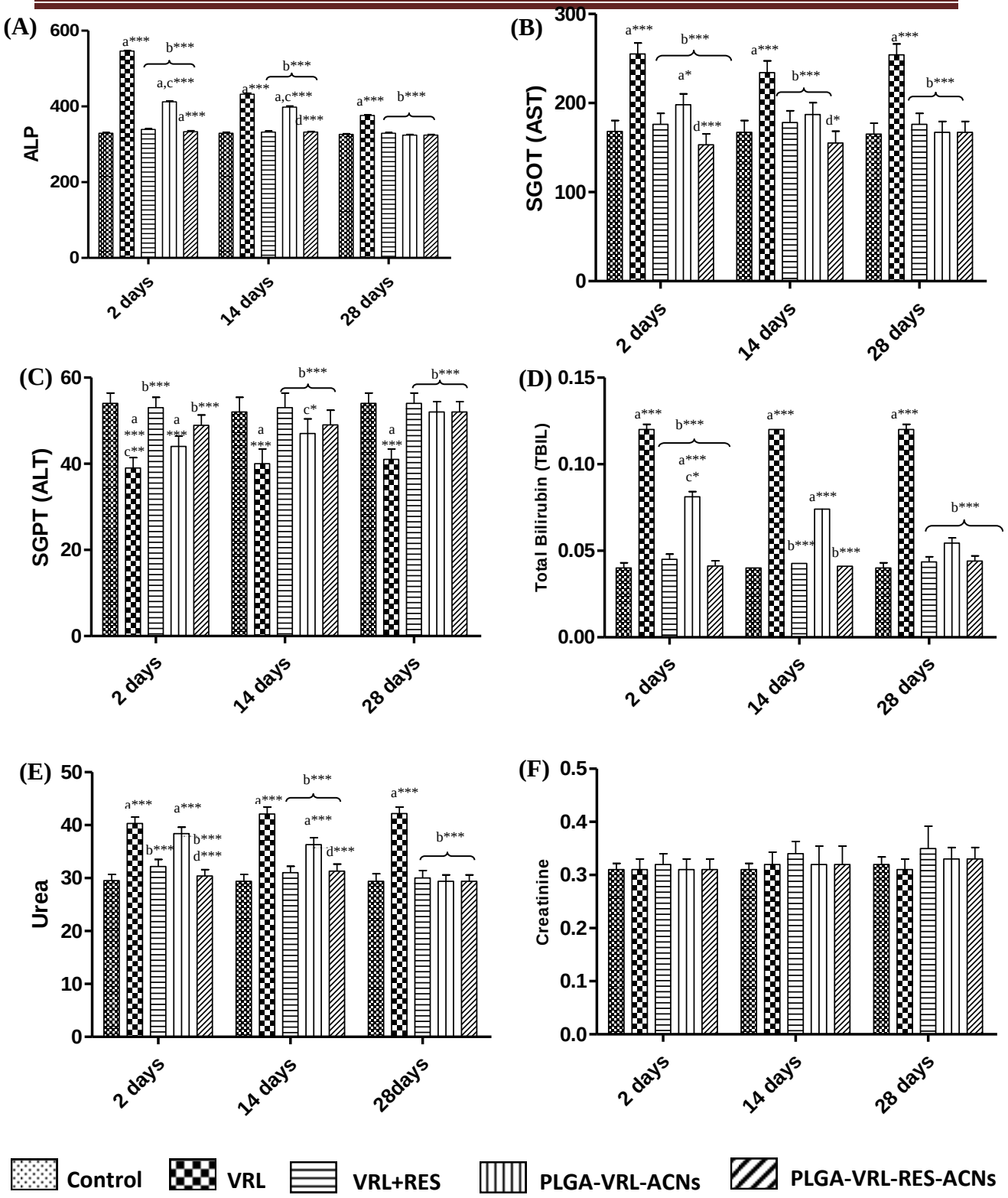

Figure 5.31: *In-vivo* toxicity of different formulations. Results were analyzed by two way ANOVA followed by bonferroni posthoc test; a: when compared with VRL; b: when compared to VRL+RES; c: when compared to GMS-VRL-RES-ACNs; ((***p< 0.0001), (**p<0.001) and (*p<0.05))

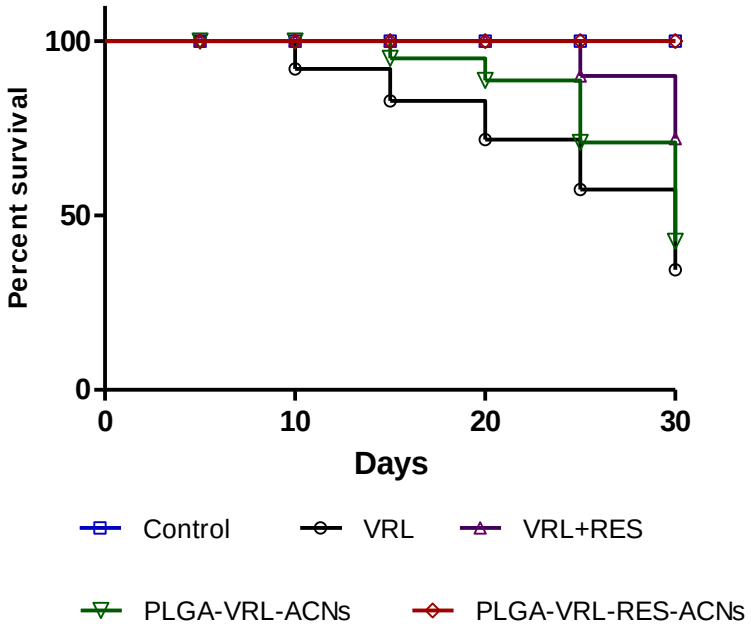

Figure 5.32: Kaplan – Meier analysis of survival of Sprague dawley rats

Figure 5.32 showed the percentage survival of animals after administration of test samples. Data suggested 100 % survival for saline and dd-ACNs treated group. Pure VRL resulted in decrease in survival from 10th day onwards leading to 50% survival in 25 days. However, combination with RES improved the survival due to proliferative and protective mechanisms of RES the same reason resulted in 100 % survival for PLGA-VRL-RES-ACNs. PLGA-VRL-ACNs also resulted in reduced survival which indicates the toxicity associated with these nanoparticles. None of the test samples displayed evidence of significant weight loss.

5.6.1.2 In-vivo anticancer studies

The anticancer effect of drug combination and dual drug loaded formulations in vivo were explored in established murine models. The animals were divided into 4 groups containing 6 mice each. All animals were administered intravenously and dynamic observations for

antitumor effects of test samples were carried out for 4 weeks. The anticancer effect was observed by measuring tumor diameter in the test animals every 6^{th} day and the tumor growth curve is shown in Figure 5.33. The result showed that tumor growth rate in group II, III and IV was slower than that of untreated group. Although the growth rate of Group III (VRL+RES) was significantly higher and similar to that obtained by VRL solution which clearly demonstrates that the synergism effect observed *in-vitro* was absent *in-vivo*. This can be attributed to the different pharmacokinetics of involving drugs. However, when the same combination was administered as nanocapsules the tumor volume (we choose three representative mice in each group) at the end of experiment was significantly reduced for PLGA-VRL-RES-ACNs treated group. The relative tumor proliferation rate was (Figure 5.34) also slower in the Group IV than that in the other groups which indicates that PLGA-VRL-RES-ACNs were able to deliver both therapeutics to the tumor at their synergistic ratio and hence an improved effect was observed at the end of the experiment. The relative tumor growth rate for VRL+RES was high compared to VRL in initial days which can be attributed to the proliferative activity of RES which vanishes with time. However, PLGA-VRL-RES-ACNs showed maximum reduction in tumor weight and hence found to be better as compared to other samples.

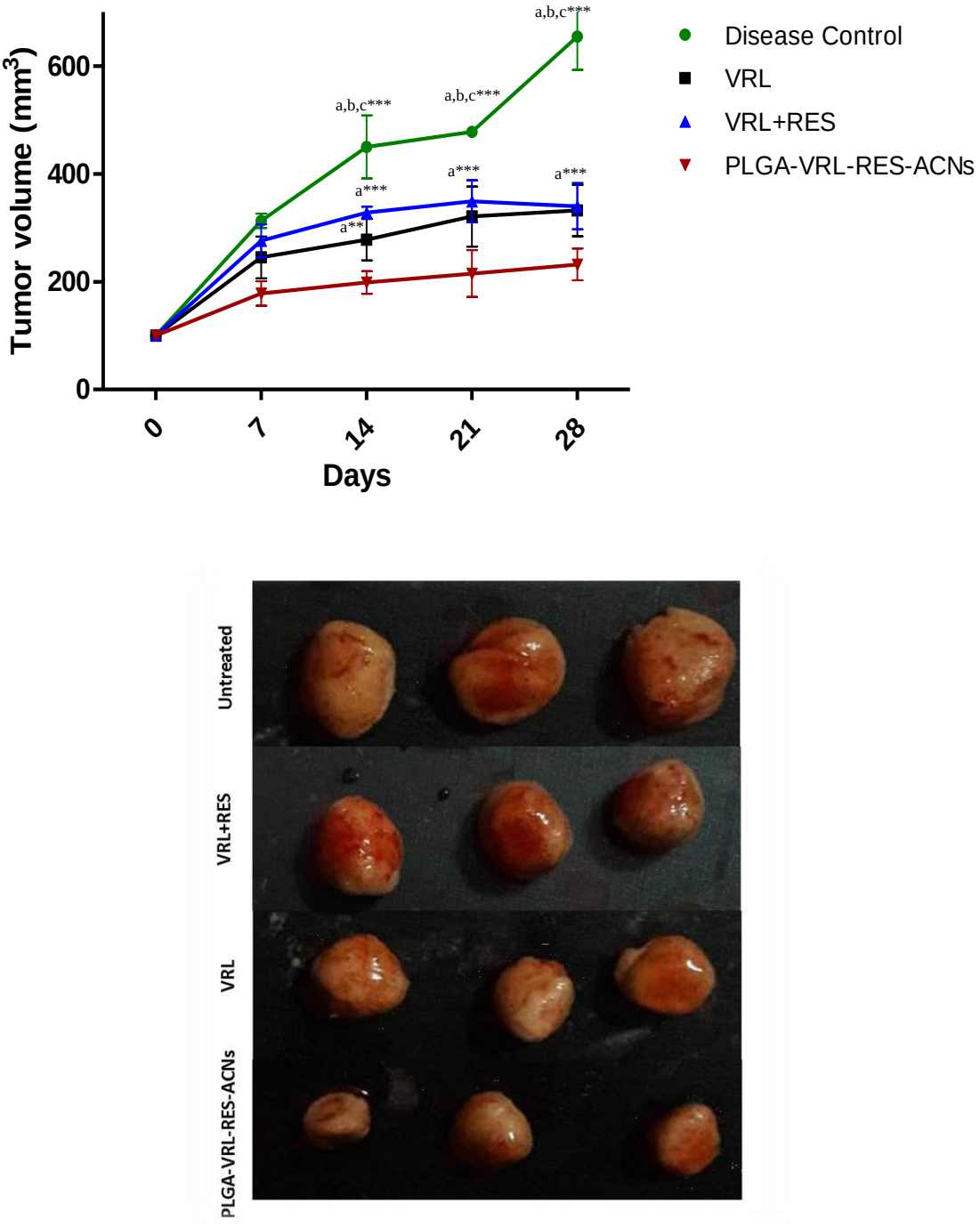

Figure 5.33: The tumor growth curve following combination therapy. Results were analyzed by two way ANOVA followed by bonferroni posthoc test ; a: when compared with PLGA-VRL-RES-ACNs, b: compared to VRL; and c: compared to VRL+RES ((***p< 0.0001), (**p<0.001) and (*p<0.05))

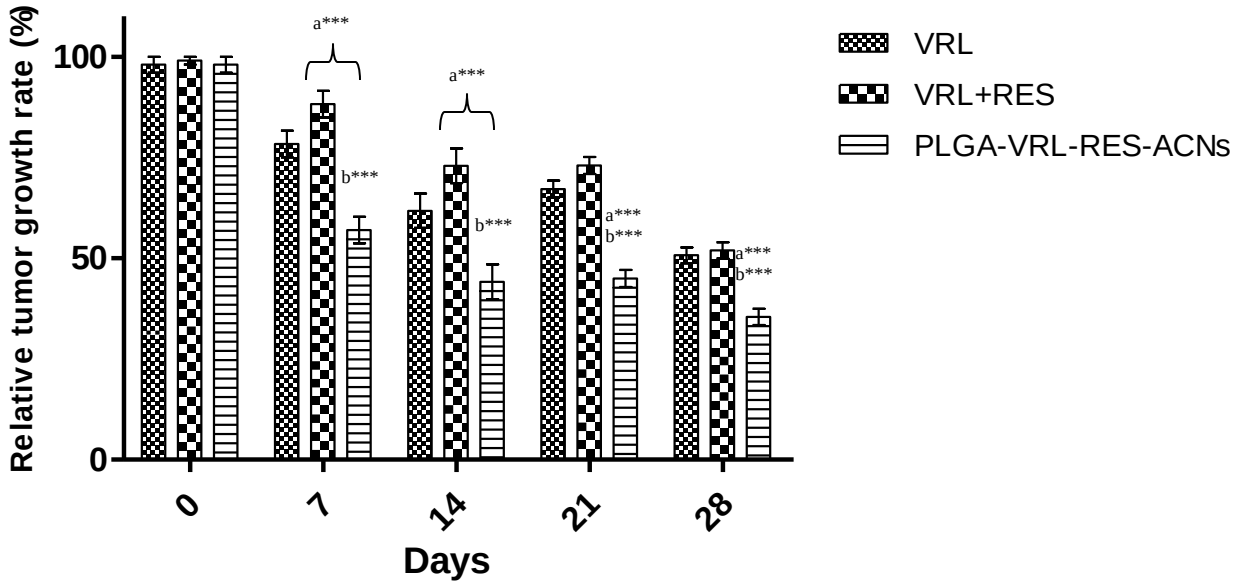

Figure 5.34: Percentage relative tumor growth rate of after treatment with VRL, VRL+RES, and PLGA-V+R-ACNs. Results were analyzed by two way ANOVA followed by bonferroni posthoc test; a: when compared with VRL, b: compared to VRL+RES; and c: compared to PLGA-VRL-RES-ACNs ((***p< 0.0001), (**p<0.001) and (*p<0.05))

The in-vivo studies confirmed the higher efficacy and reduced toxicity of combination loaded dd-ACNs. The reduction of toxicity can be attributed to the inherent properties of RES which is a natural flavanoid and exhibit antioxidant activity which improved the lifespan of population (De La Lastra and Villegas, 2007). Hence the developed dd-ACNs can be applied as potential carrier for delivery of combination of chemotherapeutics at a synergistic ratio at tumor site. In future, targeting moieties can be utilized to further enhance the therapeutic efficacy of dd-ACNs.